Master's thesis

NTNU
Norwegian University of Science and Technology
Faculty of Engineering
Department of Civil and Environmental Engineering

Lars Torgeirsson Lauvsletten

Design of Ribs in Closed Sandtraps

Master's thesis in Civil and Environmental Engineering
Supervisor: Kaspar Vereide
Co-supervisor: Ola Haugen Havrevoll
June 2021

NTNU
Norwegian University of
Science and Technology

Lars Torgeirsson Lauvsletten

Design of Ribs in Closed Sandtraps

Master's thesis in Civil and Environmental Engineering
Supervisor: Kaspar Vereide
Co-supervisor: Ola Haugen Havrevoll
June 2021

Norwegian University of Science and Technology
Faculty of Engineering
Department of Civil and Environmental Engineering

NTNU
Kunnskap for en bedre verden

Abstract

The current state-of-the-art guidelines to closed sandtraps are based on physical model studies performed in the hydraulic laboratory in the 1960s, where the model test results cannot be found, only the conclusions. This master thesis was conducted to verify the previous findings.

In this master thesis, 3D Computational Fluid Dynamics (CFD) was used to investigate two different variables in rib design for closed sandtraps, and how these affect the trap efficiency. The geometry of the CFD model is based on sandtrap no. 3 in the 960 MW Tonstad hydropower plant, and results from a physical model test have been used to calibrate and compare the numerical simulation model. Several changes to the prototype geometry are done to avoid case-specific effects on the solution, to make the results more generally valid.

Theory on sediment transport and design of closed sandtraps with ribs is presented. Theory for CFD is presented together in the methodology chapter where the numerical approach is described. For the calibration and validation, steady-state Reynolds-Averaged Navier-Stokes (RANS) simulations were conducted with two different discharges to test the validity of the CFD model. The velocity around the ribs in the CFD model was compared to the velocity measured from Particle Image Velocimetry (PIV) experiments from the physical scale model, in prototype and model scale, respectively. The comparison showed good correlation between the CFD model and the physical model.

Transient RANS simulations with sediments were carried out to investigate how the rib design affect the trap efficiency for two different variables. The first variable is the rib width, where the width is equal to the opening between the ribs. The second variable is the opening between ribs, where the rib width is fixed at 1.0 m. A total of 20 simulations were run with 0.1 mm particles injected.

Three different hypotheses were tested: 1) It is possible to further improve the rib design for closed sandtraps compared to current design recommendations, 2) The optimum distance between the ribs is 0.5 m, and 3) The optimum width of each rib is 1.0 m. The simulations showed that with the variables tested in this thesis, the rib design could not be improved. For hypothesis 2, the results from the simulations showed that the optimal distance between the ribs was 1 m. The simulations revealed that the trap efficiency was higher for simulations where the rib width was fixed at 1 m, compared to the simulations where the width varied. However, owing to the limited number of simulations run in proximity to 1.0 m, the optimal width could not be concluded. The results showed that the optimal design is 1 m wide ribs with 1 m opening between the ribs, confirming previous literature on closed sandtraps.

Sammendrag

De gjeldende retningslinjene for design av lukkede sandfang er basert på fysiske modellforsøk gjennomført i vassdragslaboratoriet på 1960-tallet, der resultatene av modellforsøkene ikke kan oppdrives, bare konklusjonene. Denne masteroppgaven ble gjennomført for å verifisere de tidligere funnene.

I denne masteroppgaven ble 3D Computational Fluid Dynamics (CFD) brukt til å undersøke to forskjellige variabler i ribbedesign for lukkede sandfang, og hvordan disse påvirker fangsteffektiviteten. Geometrien av CFD-modellen er basert på sandfang no. 3 i Tonstad vannkraftverk, 960 MW, og resultater fra et fysisk modellforsøk har blitt brukt til å kalibrere og sammenligne den numeriske simuleringsmodellen. Flere endringer av prototypgeometrien er gjennomført for å unngå case-spesifikke effekter på løsningen, og for å gjøre resultatene mer generelt gyldige.

Teori om sediment-transport og design av lukkede sandfang med ribber er presentert. Teori om CFD er presentert sammen i metodekapittelet der den numeriske tilnærmingen er beskrevet. For kalibreringen og valideringen, ble stasjonære Reynolds-Averaged Navier-Stokes (RANS) -simuleringer gjennomført med to forskjellige vannføringer for å teste validiteten til CFD-modellen. Hastigheten rundt ribbene i CFD-modellen ble sammenlignet med hastigheten målt ved hjelp av Particle Image Velocimetry (PIV) -eksperimenter fra den fysiske skalamodellen, henholdsvis i prototyp- og modellskala. Sammenligningen viste god overensstemmelse mellom CFD-modellen og den fysiske modellen.

Ikke-stasjonære RANS-simuleringer med sedimenter ble gjennomført for å undersøke hvordan ribbedesignet påvirker fangsteffektiviteten for to ulike variabler. Den første variabelen er ribbebredden, der bredden av ribben er lik åpningen mellom ribbene. Den andre variabelen er åpningen mellom ribbene, der ribbebredden holdes lik på 1.0 m. Totalt 20 simuleringer med injeksjon av partikler med 0.1 mm diameter ble kjørt.

Tre forskjellige hypoteser ble testet: 1) Det er mulig å forbedre ribbedesignet for lukkede sandfang sammenlignet med nåværende designanbefalinger, 2) Den optimale avstanden mellom ribbene er 0.5 m, 3) Den optimale bredden på hver ribbe er 1.0 m. Simuleringene viste at det ikke var mulig å forbedre designet med variablene som ble testet i denne oppgaven. For hypotese no. 2 viste resultatene fra simuleringene at den optimale avstanden mellom ribbene var 1 m. Simuleringene avslørte at fangsteffektiviteten var høyere for simuleringene der ribbebredden var fastsatt til 1 m, sammenlignet med simuleringene der ribbebredden varierte. Det er ikke mulig å konkludere med en optimal ribbebredde ettersom at det ble gjennomført få simuleringer i området nært 1.0 m. Resultatene viser at det optimale designet er 1 m brede ribber med 1 m åpning mellom ribbene, som bekrefter tidligere litteratur på lukkede sandfang.

Preface

This master thesis was written at the Norwegian University of Science and Technology (NTNU), Department of Civil and Environmental Engineering. This thesis is a continuation of the Flexible Sandtraps (FlekS) project, a collaboration between NTNU, TU Graz, and Sira-Kvina kraftselskap. The main objective of the thesis was to test the optimal rib design in closed sandtraps using numerical simulations.

I would like to thank my supervisor Adjunct Associate Professor Kaspar Vereide for the support and guidance through a challenging yet rewarding project, together with Sira-Kvina kraftselskap for rewarding the work with a scholarship. I would also like to thank my co-supervisor PhD candidate Ola Haugen Havrevoll for his support and providing data for calibration of the numerical model. I would like to thank Associate Professor Chirag Trivedi at NTNU and Dipl.-ing Dr. techn. Wolfgang Richter at TU Graz for their time and valuable help with the setup and insights to the numerical approach.

Finally, I would like to thank Arild Høydal (Sweco) for providing me with a workstation to write, in times where the university was closed owing to the Covid-19 pandemic.

Trondheim, June 2021

Lars Torgeirsson Lauvsletten

Table of contents

Abstract v
Sammendrag vii
Preface ix
1 Introduction 1
1.1 Background 1
1.2 Hypothesis 2
2 Literature review 3
2.1 CFD simulations of sandtraps 3
2.2 Design of pressurized sandtraps with ribs 4
3 Theory 9
3.1 Sediment transport 9
3.2 Sandtrap design 11
4 Methodology 15
4.1 Introduction 15
4.2 Software and hardware 15
4.3 Creating the geometry 16
4.4 Meshing 17
4.5 Governing equations 20
4.6 Numerical solution methods 21
4.7 Simulation setup for calibration and validation 31
4.8 Simulation setup for testing the hypotheses 39
4.9 Summary of verification tests for the numerical methods 40
5 Results 43
5.1 Reference case: 1m by 1 m rib setup 43
5.2 Testing cases: Variable rib and spacing widths 50
6 Discussion 51
7 Conclusion 55
7.1 Proposals for future work 55
8 References 57
Appendices 59

1 Introduction

1.1 Background

Sediments transported by the water used for energy production can cause damage to turbines and other mechanical equipment. To stop the sediments, pressurized sandtraps can be built right upstream the pressure shaft. This is the typical design of Norwegian high-head hydropower plants.

This master thesis is a continuation of the Flexible Sandtraps (FlekS) project, which was a collaboration between NTNU, TU Graz and Sira-Kvina kraftselskap, where sandtrap no. 3 at the 960 MW Tonstad power plant was a case study. The FlekS project conducted research on upgrading of existing pressurized sandtraps for operational hydropower plants, with limited downtime. One of the objectives of the project was mapping of challenges in the hydropower industry. The research revealed that hydropower plants comprising of over 25% of the total installed capacity in Norway experienced challenges related to transport of sediments, where many sandtraps did not work as intended. The challenges ranged from minor increase in wear on the mechanical components, to severe damage to turbines, and operational restrictions (Vereide et al., 2021).

Earlier research conducted at NTNU (Eggen, 1973) showed that the closed sandtraps performed better than open sandtraps, with the trap efficiency being higher. The closed sand trap is constructed with horizontal ribs to separate the flow, with higher velocity over the ribs and lower below the ribs. The velocity below the ribs should be sufficiently low to allow particles to settle and be trapped. The conclusion from the research was that new sandtraps should be built as closed sandtraps with ribs. According to Eggen (1973) physical model testing resulted in a design recommendation where the width of the rib should be equal to the opening between the ribs. The recommended rib width is suggested to be 0.8-1.0 m (Tvinnereim, 1980). However, the results from the physical model tests are not found, and this recommendation cannot be verified. The objective of this master thesis is therefore to study the optimal design of ribs and compare with the 1 m by 1 m current recommendation.

In 2019 a physical model of sandtrap no. 3 at Tonstad hydropower plant was built in the hydraulic laboratory at NTNU. The model was built in scale 1:20, where different experiments related to the FlekS project could be tested. The model was also rebuilt as a closed sandtrap with ribs, and two different rib setups were tested. Furthermore, Particle Image Velocimetry (PIV) was conducted on one setup of the rib design.

In this master thesis, Computational Fluid Dynamics (CFD) simulations will be used to investigate the optimal design of the rib setup for closed sandtraps. Calibration and validation of the CFD model will be performed by comparing steady flow simulations to the PIV experiments conducted in the physical model. Two different variables will be tested to investigate the effect they have on the trap efficiency. The first variable is the width of the ribs. The rib width is tested for two different approaches: 1) where the width is varied and 2) where the width is fixed at 1.0 m. The second variable investigated in the simulations is the opening between the ribs.

1.2 Hypothesis

This chapter presents the hypothesis of the hypotheses to be tested in this work:

1. *It is possible to further improve the rib design for closed sandtraps compared with the current design recommendations.*
2. *The optimum distance between ribs is 0.5 m.*
3. *The optimum width of each rib is 1.0 m.*

The basis for the hypotheses is that particles in a sandtrap are very sensitive to turbulence, and that the storage volume can be separated from the main flow in a more efficient way. Previous work on closed sandtraps was carried out with physical model studies in the hydraulic lab in the 1960s (Eggen, 1973). CFD simulations allow for flexible and time-efficient simulations of multiple rib designs, and it is believed that the current design can be improved.

The potentially optimum design is thought to be decreasing the space between each rib compared with the recommendations in Tvinnereim (1980) to a distance where the storage volume is affected to a lesser degree by the flow above the ribs. However, the distance between the ribs cannot be too small, as particles may theoretically hit every rib and pass the sandtrap without settling. An opening of 0.5 m between the ribs is thought to be sufficient to avoid negative effects from turbulence caused by the ribs.

The sharp edges on the upstream and downstream end of the ribs produce turbulence in the area between the ribs. If the width of the rib is decreased two issues are relevant: 1) Narrower ribs will mean less space between the upstream and downstream edges, and the flow over the rib will be disturbed by increased turbulence both over the ribs and between them, 2) The opening between the ribs is increased, allowing the main flow over the ribs to interfere with the storage volume. If the opening is kept at the same distance, narrower ribs will lead to an increased number of ribs that may result in more turbulence. The ribs cannot be too wide, as particles may only hit the ribs, and not fall into the openings. The optimum width is therefore thought to be 1.0 m as it should be a middle ground between narrow and wide ribs.

2 Literature review

2.1 CFD simulations of sandtraps

Nils Reidar Bøe Olsen and Morten Skoglund (1994) performed three-dimensional numerical simulations for a free-surface sandtrap with the program Sediment Simulation In Intakes with Multiblock option (SSIIM). The turbulence was modelled with the *k-ε* turbulence model, and the sediment concentration was calculated from the diffusion/convection equation. Physical model studies were conducted to compare to the numerical simulations. By changing the $\sigma_{\varepsilon 2}$ coefficient from 0.9 to 1.3 in the turbulence model, a more correct flow field was observed. The difference in the trap efficiency was only increased from 87.1% to 88.3% with the improved model, and it was recommended to use the original *k-ε* turbulence model for further work.

Oddmund Brevik (2013) used the CFD program STAR-CCM+ to simulate the flow in sandtrap no. 3 in Tonstad power plant in situations where free surface flow occurred. The numerical simulations were compared to field measurements from Acoustic Doppler Current Profiler (ADCP). Stationary Reynolds Averaged Navier-Stokes (RANS) simulations predicted the flow field accurately for areas with little turbulence. For areas with more turbulence, simulations using Detached Eddy Simulations (DES) gave better results. Transient simulations of filling the sandtrap with water had good correlation with measured data.

Kari Bråtveit and Nils Reidar Bøe Olsen (2015) simulated the flow in sandtrap no. 3 with the CFD program STAR-CCM+. From the CFD simulations a method for calibrating Horizontal Acoustic Doppler Current Profilers (H-ADCP) was evaluated. The study showed that Reynolds Averaged Navier-Stokes (RANS) simulation with the standard *k-ε* turbulence model failed to predict the flow field in turbulent areas, such as sudden expansions. However, in less turbulent areas the simulation predicted the flow with good accuracy for calibration and was able to predict where in the flow field the ADCPs should be installed.

Wolfgang Richter, Kaspar Vereide and Gerald Zenz (2017) presented a background of the situation at Tonstad power plant. The power plant had to be operated with restrictions due to an incident with free surface flow carrying gravel occurred in two of the sandtraps, leading to turbine damage. Three-dimensional CFD simulations were performed in scale 1:15 of sandtrap no. 3, to investigate measures to improve the trap efficiency. The simulations showed that both installing a flow diffusor just downstream the inlet and expanding the cross-section, improved the trap efficiency.

Almeland et al. (2019) performed numerical simulations of two sandtraps where multiple solutions of the Navier-Stokes equations were found. The first case was Khimti-1 power plant in Nepal, and the second was sandtrap no. 3 at Tonstad power plant in Norway. Two different CFD programs were used, SSIIM 1 and OpenFOAM. The simulations revealed that the flow pattern changed considerably depending on discretization scheme, grid resolution and turbulence model. The CFD computations were validated with field or laboratory measurements.

Rakel Næss (2020) simulated the flow in sandtrap no. 3 with the CFD software Ansys Fluent. The effect of rebuilding the sandtrap from open to closed with horizontal ribs was investigated. Steady-state RANS simulations with the realizable k-ε turbulence model were run to compare the velocities in the sandtrap with and without the horizontal plates. In addition, transient RANS simulations with sediments were performed to observe the effect the ribs had on the trap efficiency. The simulations showed that the horizontal shear-plates successfully separated the flow to decrease the velocity under the ribs, increasing the trap efficiency.

Vereide et al. (2021) conducted CFD simulations and physical modelling of sandtrap no. 3 in Tonstad power plant. The work was conducted as a part of the FlekS project, in which measures of upgrading existing sandtraps were investigated. Numerical simulations showed that several upgrades resulted in a higher trap efficiency. The upgrades were (1) sandtrap rebuilt with ribs, (2) flow calming structures at the inlet, (3) baffles paired with an automatic sluicing system and (4) geometrical improvements to reduce turbulent kinetic energy. Physical model testing at TU Graz showed that rebuilding the sandtrap with ribs increased the trap efficiency from 0% to 90% for particles in the range 0.3 to 1.0 mm. Physical model testing at NTNU with d_{50} equal to 3 mm showed no difference in the trap efficiency with or without ribs. An innovative solution for upgrading sandtraps in conjunction with a surge tank was also introduced.

2.2 Design of pressurized sandtraps with ribs

Mattimoe et al. (1964) conducted physical model testing of a sandtrap and a rocktrap in the Jaybird Tunnel, part of the power system of the Jaybird Powerhouse belonging to the Upper American River Project (UARP). The model experiments were initiated after two incidents where rocks were heard transported through the penstocks and turbines, and subsequent dewatering and inspections showed that the sandtraps did not perform as intended. Two models, one of a rocktrap and one of a sandtrap were built in geometric scale of 1:12. Four tests were carried out; the first test was on the original sandtrap to test the validity of the physical model, the second tested corrective measures to the original sandtrap, the third test was a longer sandtrap of the original configuration, and the fourth test was research to develop a new sandtrap design.

The original Jaybird sandtrap was built as a vertical expansion of the tunnel by gradually lowering the invert, with cells divided by baffle walls where the sediments could settle. The results from the original design showed that sediments entering the traps encountered highly turbulent flow caused by vortices. The turbulent flow conditions would keep most sediments from settling. Sediments were observed lifted over the baffle walls and into the main flow transporting them through the trap, confirming the findings from the inspections of the prototype. During test phase two, a three-part horizontal staging was placed over the cells at the level of the tunnel invert. The staging consisted of an opening where the particles could fall freely, followed by a section of rounded steel bars with a given spacing, and lastly a fully covered section. From the model testing it was observed that the horizontal staging successfully carried the shear of the main flow, separating it from the storage volume, creating calm conditions in the cells. An opening between the baffle walls and the horizontal staging allowed excess sediments to fall into the next cell, leading to nearly complete filling of each cell. The testing with the horizontal staging led to a new design of sandtraps called the CELSEP trap. The basic configuration of the CELSEP trap can be seen in figure 2.1, based on Mattimoe et al. (1964):

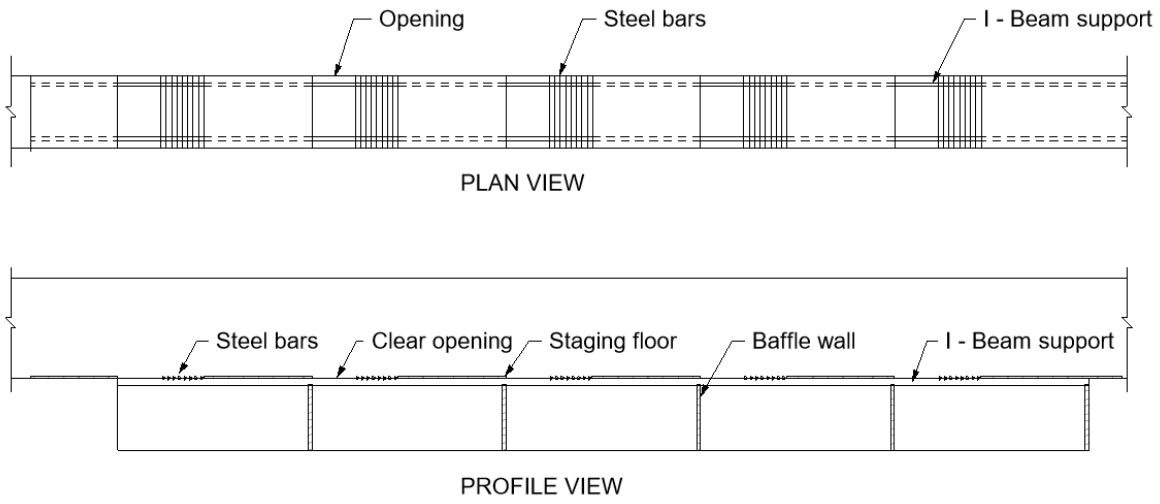

Figure 2.1: Layout of the CELSEP trap, where the dimensions are in feet.

The CELSEP trap resulted in a greatly improved trap efficiency while also having much lower head loss compared to the original constructions, owing to no expansion of the tunnel cross-section, except in the invert. The results from the physical model testing led to a new state-of-the-art design for future sandtrap-projects in the UARP power system.

Eggen (1973) investigated the connection between sediments left on the tunnel invert after construction and sediments found in the subsequent sandtraps, to establish recommendations and new design criteria for future sandtraps. Sediment samples of material left from construction from multiple hydropower plants revealed that the grain distribution curve was similar between the power plants. On average 20% of the material found consisted of fine particles with a diameter $d < 0.3$ mm. Particles with a diameter in the range $d < 0.3$ mm – 0.6 mm dependent of flow velocity are considered suspended load. Conventional sandtraps in Norwegian hydropower plants are usually built too short, in combination with poor flow conditions owing to the placement and/or geometry of the sandtrap, to collect particles smaller than 0.3 mm. The length of the short traps is typically 30 – 60 m. Longer sandtraps with lengths of roughly 150 m with good flow conditions may allow settling of finer particles carried in suspension. However, the courser particles transported as bed load will settle in the upstream part of the sandtrap, and will lead to increased flow velocity from continuity, that may reintroduce the finer particles to the flow. In figure 2.2, a basic layout of two short sandtraps is presented, based on Eggen (1973).

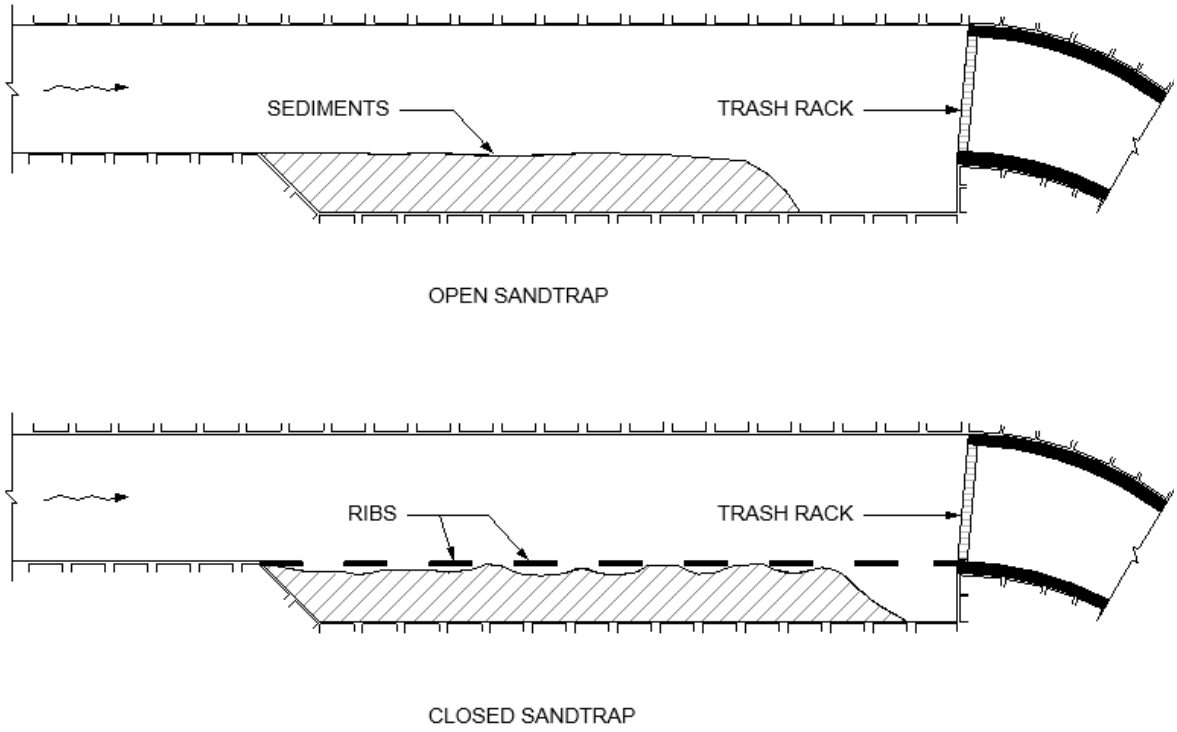

Figure 2.2: Basic layout of open and closed sandtraps.

The sandtrap was typically placed just upstream the pressure shaft. The cross-sectional area was expanded in the horizontal and vertical direction to reduce the flow velocity, to allow particles to settle. Extra expansion in the tunnel invert made room for the storage of sediments. Physical model studies showed that closed sandtraps with ribs separated the main flow and the storage volume and improved the trap efficiency of the sandtrap. The expansion in the tunnel roof and walls proved to be unnecessary for closed sandtraps. The model studies showed that the width of the ribs and opening between them should be of the same magnitude, 0.8-1.0 m.

Kaspar Vereide (personal communication, 09.06.21) provided information about sandtraps in the Karahnjukar power system in Iceland. Three sandtraps are built in the head race tunnel to collect rocks and gravel, in addition to debris from rockfall and erosion. The traps are constructed similarly to the CELSEP trap in the Jaybird tunnel, where the invert is lowered and divided into cells by vertical walls, and the regular cross-section remains unchanged. The main flow is separated from the storage volume by a three-part horizontal decking: The first quarter is an open space for debris to fall into the cell, the second quarter consists of 32 mm steel rebar with 200 mm spacing, and the last half is covered by wooden planks. Sediment transport between the cells is allowed by two small openings at the bottom of each wall, allowing for full utilization of the storage capacity.

Richter et al. (2020) performed physical model studies of sandtrap no. 3 in the 960 MW Tonstad hydropower plant as a part of the FlekS project. The physical model was built in scale 1:36.67, and the sand particles were scaled 1:1 with the prototype, resulting in

particle sizes between 0.3 and 1.0 mm. The physical model revealed that for the current prototype situation, the trap efficiency was 0%. The model was then rebuilt with ribs in only the downstream end of the sandtrap. The rib section consisted of a ramp with 8% inclination and five ribs, where the first and last rib were connected to the ramp and the weir, respectively. The ribs tested had a width of 1 m and opening of 1 m in prototype scale, following the recommendations of (Tvinnereim, 1980). The experiments where the model was rebuilt as a closed sandtrap with ribs in the downstream section resulted in a trap efficiency of 90%.

The physical model studies referenced by Eggen (1973), and the physical model testing performed by Richter et al. (2020), reveal that research has been concentrated on the effect of installing ribs in sandtraps, and not the actual design of the ribs. As only the conclusions from the model studies carried out in the 1960s are known, and not the results, there is no knowledge of the volume of rib designs tested to result in the recommendation by Tvinnereim (1980) of 0.8-1.0 m rib width and opening. The flexibility of CFD simulation allow for testing multiple setups of rib design, to investigate the optimal width and opening, and if the design can be further improved.

3 Theory

3.1 Sediment transport

3.1.1 Suspended load and bedload

Sediment transport for hydropower purposes is divided into two types of transport, suspended load and bedload. In suspended load, the particles are carried in suspension, without contact with the bed. In bedload, the particles are frequently touching the bed, moving by gliding, rolling or saltating along the bed. There is no clear limit for the transition between bedload and suspended load. A practical limit for suspended load in open surface flow is when the shear velocity is larger than the particles' sinking velocity (Fergus et al., 2010). Research conducted at NTNU on pressurized flow showed that particles with a diameter d < 0.3– 0.6 mm in general are transported in suspension, but is dependent on the flow velocity (Eggen, 1973). Pressurized sandtraps with ribs are only expected to capture bed load. The limit between how particles are transported as suspended and bed load is therefore of particular interest for these sandtraps.

3.1.2 Shields diagram

The limit between a moving and a settled particle is of particular interest for sandtrap design. The movement of particles can be predicted by calculating the shear stress at the bed. Shear stress over a critical value τ_c will allow for movement of a given particle diameter. Shields parameter is the dimensionless critical shear stress used to calculate the motion of a particle and is given by:

$$\tau^* = \frac{\tau_0}{(\rho_s - \rho_w) g d_s} \tag{1}$$

where τ_0 is the shear stress at the bed [N/m^2], ρ_s is the particle density [kg/m^3], ρ_w is the density of water [kg/m^3], g is the gravitational acceleration [m/s^2] and d_s is the particle diameter [m].

Shields diagram adapted from (Schwimmer, 2007) is presented in figure 3.1. Shields curve is a function of the Shields parameter and the boundary Reynolds number, Re^*, described in the following equation (Olsen, 2017):

$$Re^* = \frac{u_* d_s}{\nu} = \frac{d_s \sqrt{\frac{\tau_0}{\rho_w}}}{\nu} \quad (2)$$

where u_* is the shear velocity [m/s] and ν is the kinematic viscosity of water [m^2/s].

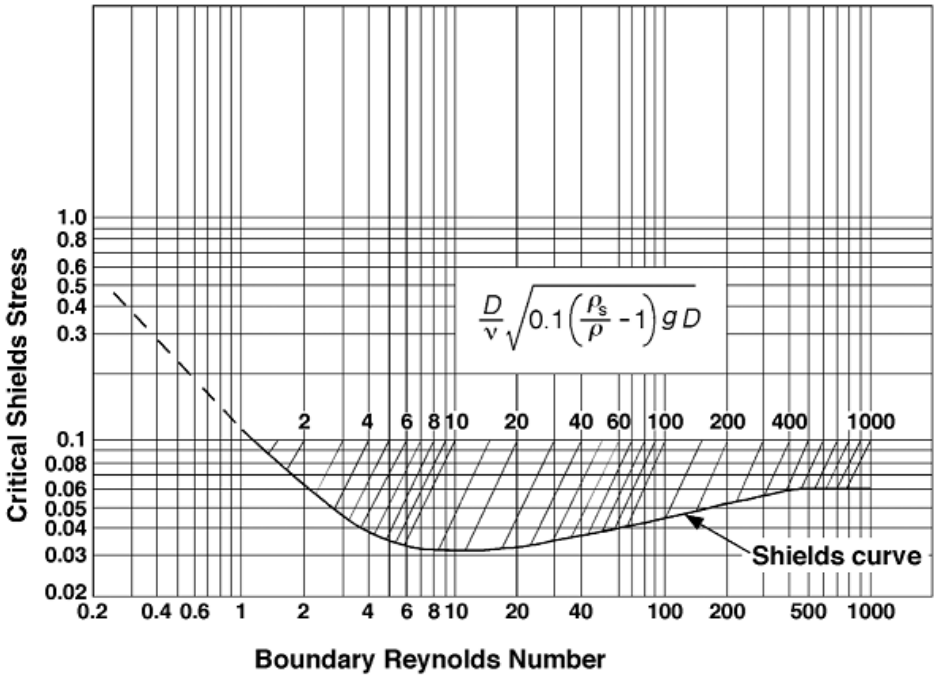

Figure 3.1: Shields diagram.

Equation (1) in combination with Shields diagram can be used to calculate the critical shear stress for movement of a particle on the bed if the particle size is known, or calculate the particle diameter that will not be eroded (Olsen, 2017). Shear stresses above the critical value given by Shields curve will lead to erosion, while lower values will not cause particle movement.

3.1.3 Sand movement in tunnels

The requirements of particle movement described by the Shields diagram is based on open channel hydraulics, and not pressurized flow in tunnels. However, since the flow conditions for both canals and tunnels are well understood, it is a reasonable assumption that the same conditions should apply to tunnels, with some modifications (Lysne, 1969). Several equations describing the limiting tractive force on sand particles in flowing water exist, including Shields equation. Owing to the similarity between the equations (Lysne, 1969), they can be expressed as:

$$d = \frac{\tau_0}{(\gamma_s - \gamma_v)\, C} \quad (3)$$

where *d* [m] is the particle diameter, τ_0 is the shear stress at the bed [N/m^2], γ_s and γ_v is the specific weight of sand and water [N/m^3], respectively, and *C* is a coefficient [-]. Furthermore, the equations for the bed shear stress and Manning's formula are introduced:

$$\tau_0 = \gamma_v R S \tag{4}$$

$$V = \frac{1}{n} R^{\frac{2}{3}} S^{\frac{1}{2}} \rightarrow S = \frac{n^2 V^2}{R^{\frac{4}{3}}} \tag{5}$$

Where *S* is the longitudinal slope [m/m], *R* is the hydraulic radius [m], *V* is the water velocity [m/s], and *n* is Manning's roughness coefficient [s/m$^{1/3}$]. For tunnels, the hydraulic radius is substituted:

$$R = K A^{\frac{1}{2}} \tag{6}$$

Where *K* is a coefficient [-], and *A* is the cross-sectional area [m^2]. Combining equations 3, 4, 5, and 6 results in an expression for the critical particle diameter in tunnels (Lysne, 1969):

$$d = \frac{\gamma_v}{\gamma_s - \gamma_v} \frac{n^2 V^2}{C' A^{1/6}} \tag{7}$$

Where $C' = \frac{C K^{1/3}}{n^2}$ is a coefficient with an approximate value of 130 in metric units (Lysne, 1969).

3.2 Sandtrap design

3.2.1 Background

Sediments can enter the hydropower system from various sources like reservoirs, rivers, and brook intakes. In Norwegian hydropower, the most common design of waterways are unlined tunnels, owing to good and solid rock quality. Under construction, some of the blasted rock and finer masses are used to create a temporary road for transportation of masses out of the tunnel. After the construction is complete, the masses left on the tunnel invert will for most situations be partly removed, or completely in some cases, depending on an economical perspective (Eggen, 1973). Material left on the tunnel invert will be transported by the water towards the turbines, and data from four Norwegian hydropower plants showed that from the material left on the invert: 25% was not transported, 25% was transported in suspension, and 50% was transported as bedload

(Eggen, 1973). Owing to the conventional sandtrap in Norwegian hydropower being too short to trap suspended load, 25% of the material is transported through the turbines (Eggen, 1973). A stable armor layer where larger particles protect finer particles from further erosion will be formed after some production time that will limit the transport of materials, but forming the layer may take several years (Eggen, 1973). Increased flow rate by upgrading current turbines, and unsteady flow from peak production, may disturb the layers that were stable for a lower flow rate, and lead to increased erosion.

Sediments should be stopped before entering the pressure shaft as the particles can cause damage to the turbine by erosion, clogging or single-point damage. Smaller particles can lead to erosion and clogging, resulting in lower efficiency and increased need for maintenance, while larger particles can cause single-point damage resulting in start-up cavitation (Vereide et al., 2017).

3.2.2 Flow conditions

Calm flow conditions in sandtraps are important to allow trapping of sediments and avoid further transport. Inspections at Norwegian hydropower plants and physical model tests have revealed that common sandtraps are not working as intended (Eggen, 1973). The location of the sandtrap in relation to upstream curves and bends is important for the trap efficiency, as they may lead to uneven velocity distribution in the sandtrap, where the outer curve has a higher velocity. If the sandtrap is placed near or in tunnel junctions, the flow conditions will be affected by the formation of eddies and increased turbulence (Eggen, 1973). As described in section 3.2.1, sandtraps in Norwegian hydropower systems are commonly placed right upstream the pressure shaft, downstream of the surge shafts. This placement is beneficial for trapping sediments as mass oscillations from the surge shaft will not disturb the flow in the sandtrap (Vereide et al., 2017). To improve the trap efficiency, the sandtrap should be placed 100 – 200 m downstream of curves and tunnel junctions, resulting in calm and uniform flow conditions (Eggen, 1973). The transition from the headrace tunnel to the sandtrap should not be too sudden. Short and sudden expansion from the tunnel cross-section to the sandtrap may lead to the flow separating from the walls and roof, causing turbulence (Eggen, 1973). The horizontal expansion angle should not exceed 4° for the walls, and the vertical expansion angle should not exceed 8° for the roof, while the transition in the invert can be abrupt (Eggen, 1973). Sediments settled in the sandtrap will disturb the flow conditions in open sandtraps but will be avoided with closed sandtraps owing to the horizontal ribs separating the main flow (Eggen, 1973).

3.2.3 Design

The common practice to construction of sandtraps in Norwegian hydropower plants is an expansion of the headrace tunnel immediately upstream the pressure shaft and downstream of an eventual surge shaft or chamber. This placement is considered optimal owing to the pressure shaft being steel lined, meaning that no new sediments will enter the waterway after the sandtrap. This layout allows the construction of unlined tunnels where sediments can be left on the invert after construction, and the tunnel itself can function as a sandtrap (Vereide et al., 2017).

The expansion of the sandtrap provides a larger cross-section resulting in a lower flow velocity, in addition to storage volume for trapped sediments. The expansion should be constructed without abrupt angles as described in section 3.2.2, to assure good flow conditions. The sandtraps are commonly built as either open or closed sandtraps.

Physical model tests performed in the hydraulic laboratory discovered that closed sandtraps had a better trap efficiency compared to open sandtraps and could obtain almost full capacity when fitted with ribs in only the upstream part of the sandtrap (Eggen, 1973). The recommended design for ribs is that the rib width and opening should be of the same magnitude, where the width is 0.8-1.0 m (Tvinnereim, 1980). The model tests showed that expansion in the walls and roof to reduce the velocity was not needed for closed sandtraps, as the bedload was still trapped in the storage volume (Eggen, 1973).

The design of sandtraps usually consists of picking a particle size that should not be exceeded, where a trap efficiency is decided based on experience. The typical particle size for Norwegian hydropower plants allows for particles with diameter 1-2 mm to pass the turbines (Vereide et al., 2017). The particle sizes will vary depending on factors like the origin of the sediments, the mineralogy and sediment load. The design of sandtraps based on experience and without further research like physical model testing, results in many sandtraps not working as intended (Eggen, 1973).

Economical optimization regarding the design of sandtraps should include several factors summarized by Eggen (1973):

- The amount of material left in the head race tunnel after construction.
- Sediment transport from brook intakes and/or reservoirs.
- The floor area of the tunnel invert, to assess the amount of material left.
- Maintenance schedule and emptying of the trapped sediments.
- Construction of longer sandtraps to allow for some trapping of material transported in suspension.
- Expectation and risk of mechanical wear on turbines and other installations.

3.2.4 Trap efficiency

The trap efficiency η is used as a measure to describe the functionality and performance of a sandtrap, where a higher trap efficiency relates to a well-functioning sandtrap (Paschmann, 2018). The desired trap efficiency of a sandtrap should be decided in the planning stage of construction and should be determined by operational demands regarding turbine and mechanical wear, and intended sediment removal intervals (Paschmann, 2018). Several approaches of determining trap efficiency exists, and the approach is chosen based on the requirements from the planning stage. In a particle-size approach, a critical particle size d_{cr} is decided based on requirements from the power plant operator or the turbine manufacturer, and all particles larger than d_{cr} should be trapped (Paschmann, 2018). In a mass or concentration related approach, particle sizes are not considered in the calculations, only the total reduction of sediments. The mass related approach calculates the trap efficiency by the sediments entering and leaving the sandtrap per unit time. The trap efficiency for the concentration related approach is determined by the concentration difference between the inlet and the outlet of the sandtrap. In this thesis, the simulations will be performed with a uniform particle size distribution. The trap efficiency can be determined using equation (8), where m is the mass injected or escaping the sandtrap (Ranga Raju et al., 1999):

$$\eta = 1 - \frac{m_{s,out}}{m_{s,in}} \tag{8}$$

4 Methodology

4.1 Introduction

Hydraulic design and research of hydraulic problems have previously been solved with physical model studies. The physical models may require large floor areas in a laboratory, and the construction is often time-consuming and expensive. Therefore, the models are often scaled down to a size that is appropriate from an economical perspective, and available space. Downscaling may introduce scale effects that result in non-identical force ratios between the model and prototype (Paschmann, 2018). Scale effects can be related to surface tension in experiments with free surface flow, or cohesive forces between particles. In contrast, CFD-modelling is not subjected to scale effects, and can solve complex hydraulic situations of fluid and sediment flow.

Computational Fluid Dynamics (CFD) is the concept of solving numerical models for fluids using a computer. CFD simulation has several advantages compared to physical model studies, as it is very time and cost efficient. The ability to make changes to the model and simulation settings, provide good flexibility and ease of use. However, CFD-modelling has some limitations as it is based on several approximations and simplifications and may not always provide reliable results. As described in section 2.1, the findings of Almeland et al. (2019) showed that the solution of a simulation can vary depending on the numerical approach and methods applied. Physical model studies can therefore be needed to calibrate and test the validity of the CFD model.

In this thesis the CFD model will be calibrated against data from physical model studies to obtain a valid model. The physical model experiments were performed in the NTNU Hydraulic Laboratory as part of the Flexible Sandtraps project.

4.2 Software and hardware

Ansys Fluent is a commercial 3D fluid simulation software. The software package consists of multiple programs to complete the simulation from start to finish. The programs are user-friendly with a step-to-step interface, making the entire process easy to follow.

Ansys Fluent has shown to give good results when simulating the flow in pressurized sandtraps, both with and without sediments (Næss, 2020). The academic version of Ansys Fluent 2021 R1 have been used to perform the simulations. The academic version has some limitations that will be described in later sections.

The simulations have been performed on a Lenovo Thinkpad with 16 GB memory and Intel®Core™ i5-8365U processor with 1.9 GHz and 4 cores. In addition, due to the transient simulations being time consuming, a private desktop was also used to run simulations. The desktop has 16 GB memory and an Intel®Core™ i7-4790K processor with 4 GHz and 4 cores.

4.3 Creating the geometry

The model used in the simulations is created with the 3D modelling software Ansys SpaceClaim. The model is created as a simplified geometry of sandtrap no. 3 at Tonstad hydropower plant, based on construction drawings provided by Sira-Kvina kraftselskap. The drawings are found in Appendix A.

A simplified geometry has been selected to make the results more generally applicable. The Tonstad sandtrap has several site-specific features that may influence the results. The geometry has the same cross-sectional area as the expanded area of sandtrap no. 3 in Tonstad. The similar geometry is used as a measure to be able to compare the flow field in the numerical model with PIV experiments carried out in the hydraulic laboratory. The model used for the initial simulations to determine a sediment diameter that gives a trap efficiency around 50 percent, is shown in figure 4.1.

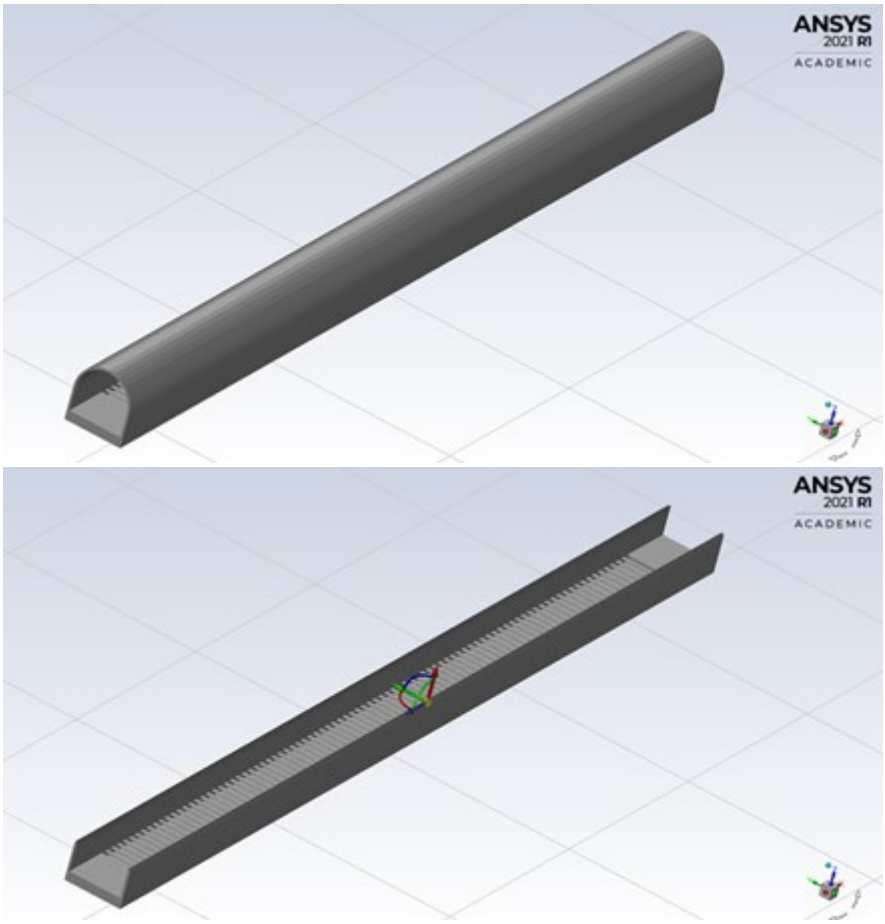

Figure 4.1: Sandtrap model.

The inlet and outlet sections have been extended by 10 m beyond the rib section to obtain steady flow conditions, and the invert has been raised 1.5 m to be flush with the top of the ribs in the sandtrap. The length of the rib section is 180 m, resulting in a total length of 200 m for the entire model. For the initial simulation, the sandtrap is constructed with ribs covering the full width of the model. The first and last ribs are

placed immediately after the invert is lowered, to avoid gaps that may affect the flow. The ribs have a length of 1 m in the x-direction and a spacing of 1 m, according to current design recommendations. The thickness is 0.16 m to represent the scale of the ribs used in the physical model in the hydraulic laboratory. For the simulations running different rib designs, the original geometry is unchanged, and the ribs are updated in SpaceClaim.

4.4 Meshing

Meshing in CFD is the concept of dividing the fluid domain into smaller cells or elements to create a discretized representation of the domain and solving finite volume equations for each cell (Paschmann, 2018). The accuracy and convergence of a CFD simulation is affected by the number of cells and the quality of the mesh (Olsen, 2017). A finer mesh, or grid, may give more accurate results compared to one with fewer cells, but will demand more computational resources. An important aspect of the meshing process is therefore to find a mesh resolution and quality that provides the needed accuracy with the resources available.

The quality is dependent on the grid characteristics non-orthogonality, aspect and expansion ratio, and skewness. The orthogonality is a measure of how much the angle between adjacent element faces deviates from an optimal angle. The optimal angle depends on the elements in the grid and is 90° for quadrilateral- and 60° for triangular elements. The angles between the elements should not be below 45° or above 135°, as the grid would be considered very non-orthogonal. Low non-orthogonality is associated with more rapid convergence, and in some cases better accuracy (Olsen, 2017). The orthogonality of the mesh is reported as a value between 0 and 1, where 0 is very non-orthogonal, and 1 is orthogonal. Figure 4.2 shows two elements used to describe the aspect and expansion ratio.

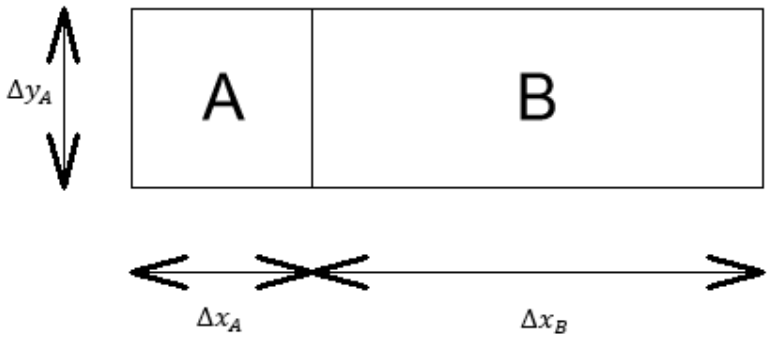

Figure 4.2: Expansion and aspect ratio.

The expansion ratio of these cells is given as $\Delta x_A/\Delta x_B$, and should ideally be lower than 1.2 to avoid calculation problems. The aspect ratio is given as the relationship of the cell width and length, $\Delta x_A/\Delta y_A$. Low aspect- and expansion ratio is preferred, as large values may lead to slow solution and convergence problems (Olsen, 2017).

The final quality measure of the grid is the skewness ratio. The skewness is the difference between the shape of the cell compared to the ideal cell shape, reported as a value between 0 and 1, where 0 is the ideal shape. Highly skewed cells can decrease accuracy and lead to unstable solutions (Ansys Fluent).

The mesh can be created with elements of different shapes, and the choice depends on several factors such as geometry, required accuracy, and computational resources. The available cell shapes in Ansys Fluent is shown in figure 4.3 (Ansys Fluent).

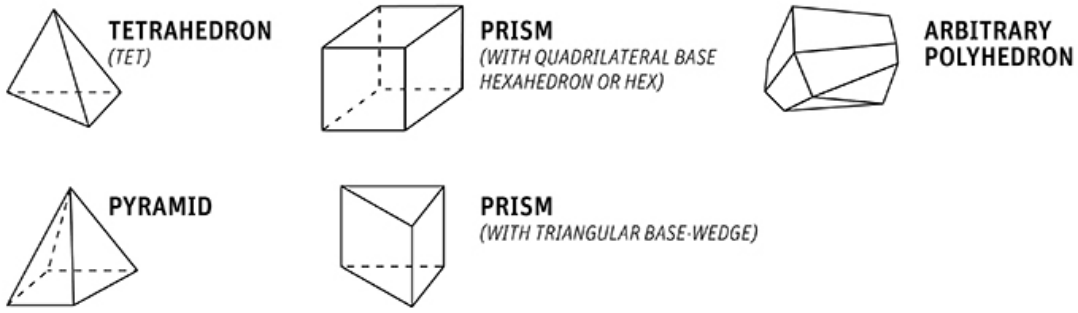

Figure 4.3: Element shapes available in Ansys Fluent

The *Volume Extract* tool is used to extract the internal fluid volume from the model in SpaceClaim. The extracted volume is exported to Ansys Fluent, where the meshing is performed. The model is split in half along the x- and z-axis by a *symmetry plane* to decrease the number of elements used, and to improve calculation time. The academic version of Ansys Fluent allows meshing of up to 512 000 elements. The *symmetry plane* mirrors the model and therefore allows for greater accuracy by increasing the cell density used in the simulations.

Before the mesh is generated, *Named Selections* are created to separate the different boundaries of the model. There are several types of named selections with different properties associated with the given type. Named selections are applied for the inlet, the outlet, the symmetry plane and the bed and walls.

The mesh is created using polyhedral cells and recommended values to keep within the limitations of the academic version. Once the mesh has been generated, Ansys Fluent automatically performs a mesh check according to the different quality measures and suggests improvements if needed. The number of elements and nodes used for the initial simulation is shown in figure 4.4.

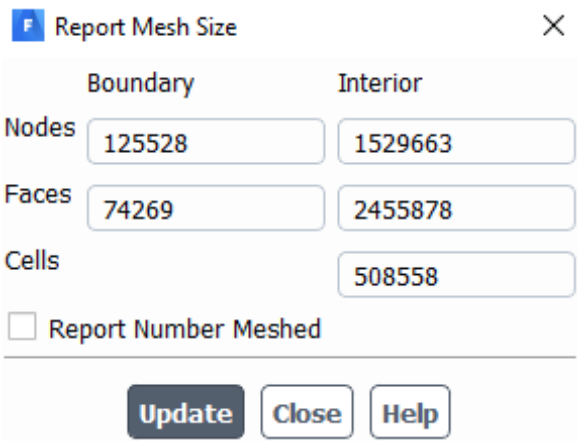

Figure 4.4: Mesh size in initial simulation.

An overview of the mesh used for the original rib design simulations is shown in figure 4.5. The same procedure is followed for all the simulations, but the meshing process must be repeated for every simulation. The mesh used for the simulations is the finest resolution that can be applied within the limitations of the academic license of Ansys Fluent. For the simulations where the rib design is changed, experimenting with minimum cell sizes is necessary to stay under the maximum number of cells allowed. Ideally, a mesh independence study should be performed, where the solutions of simulations with an increasing number of cells are compared. A mesh independence study is not performed as all the meshes are created with the maximum number of cells available.

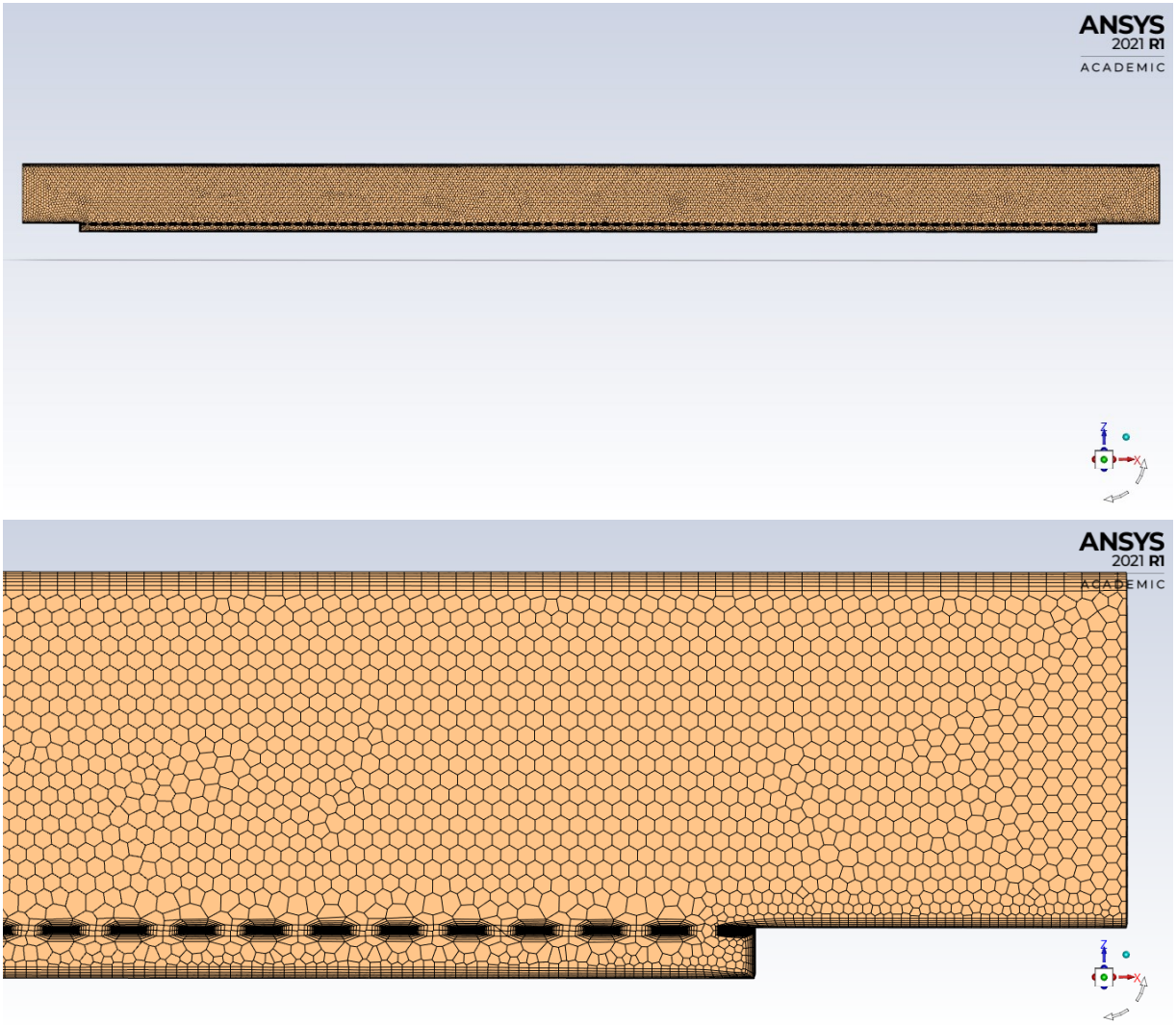

Figure 4.5: Mesh overview.

4.5 Governing equations

Numerical simulation using CFD is based on the three conservation laws of physics: conservation of mass, Newton's second law and conservation of energy. Expressing these laws mathematically result in the governing equations: the continuity, the momentum, and the energy equations (Versteeg & Malalasekera, 2007). The conservation of mass, where the inflow rate is equal to the outflow rate is described by the continuity equation in three dimensions:

$$\frac{\partial \rho}{\partial t} + \frac{\partial (\rho u)}{\partial x} + \frac{\partial (\rho v)}{\partial y} + \frac{\partial (\rho w)}{\partial z} = \frac{\partial \rho}{\partial t} + \frac{\partial u_i}{\partial x_i} = 0 \qquad (9)$$

Where ρ is the density [kg/m^3], t is the time [s], u, v, and w are the flow velocities in each direction [m/s]. The directional flow velocities are denoted u_i combined. For incompressible flow, the density ρ is constant, and the expression can be simplified to:

$$\frac{\partial u_i}{\partial x_i} = 0 \tag{10}$$

The momentum equations, also known as the Navier-Stokes equations, can for three dimensions be expressed as:

$$\rho \frac{\partial u_i}{\partial t} + \rho u_j \frac{\partial u_i}{\partial x_j} = -\frac{\partial p}{\partial x_i} + \mu_t \frac{\partial^2 u_i}{\partial x_j^2} \tag{11}$$

The left-hand side of equation 11 represents a transient and a convective term, and the right-hand side represents a pressure and a diffusive term. Where p is the pressure in [Pa] and μ_t is the turbulent eddy viscosity [Ns/m^2].

The energy equation is based on the first law of thermodynamics, which states that the rate of change of energy of a fluid particle is equal to the work done on the particle and the rate of heat addition (Versteeg & Malalasekera, 2007). Thermal investigation is not relevant for this thesis and will not be discussed further.

4.6 Numerical solution methods

The Navier-Stokes equations need to be discretized in order to solve them with a computer. The discretization can be performed by the finite difference, finite element, and the finite volume methods. For Ansys Fluent the finite volume method is used and will be introduced in the following sections.

4.6.1 Discretization of the Navier-Stokes equations

Steady state of a general quantity Φ is governed by the convection-diffusion equation (Olsen, 2017):

$$u_i \frac{\partial \Phi}{\partial x_i} = \frac{\partial}{\partial x_i}\left(\Gamma \frac{\partial \Phi}{\partial x_i}\right) \tag{12}$$

Where the left-hand side of the equation is the convective term, and the right-hand side is the diffusive term with a turbulent diffusion coefficient, Γ [-]. Discretization is the process of transforming the partial differential equation to an equation where the variable in each cell is a function of the same variable in neighboring cells (Olsen, 2017). The discretized transformation of equation 12 can be regarded as weighted averages of the neighboring cells:

$$\Phi_p = \frac{a_w \Phi_w + a_e \Phi_e + a_n \Phi_n + a_s \Phi_s}{a_p} \tag{13}$$

In equation 13 *a* is the weighting factor of the cell and the denotations refer to the neighboring cell in a direction. For a three-dimensional calculation, a top and bottom cell is added to the molecule, resulting in six neighboring cells (Olsen, 2017). The discretization molecule is shown in figure 4.6:

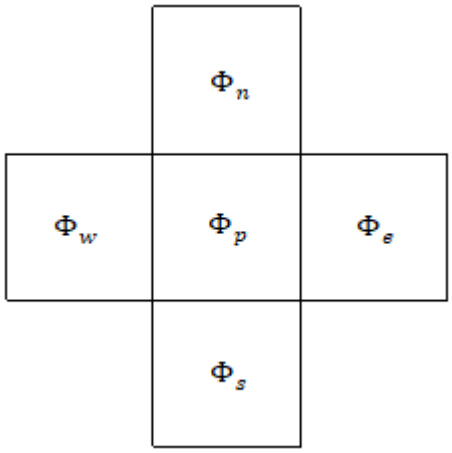

Figure 4.6: Discretization molecule.

In Ansys Fluent the discrete value of Φ is stored in the center of the cell, but in addition, values at the cell faces are needed to solve the convective terms. The values at the cell faces are interpolated from the cell centers using an upwind scheme (Ansys Fluent).

Upwinding means that the value of a cell surface is derived from a cell upwind of the control cell. The First Order Upwind scheme derives the surface values from one cell upstream the control cell. The scheme assumes that the quantities in the center of the cell holds through the entire cell, meaning that the face quantity is equal to the cell quantity, resulting in the face quantity of the cell is equal to the quantity in the upstream cell (Ansys Fluent). The Second Order Upwind scheme uses two upwind cells to estimate the face quantity at the control cell, as shown in figure 4.7:

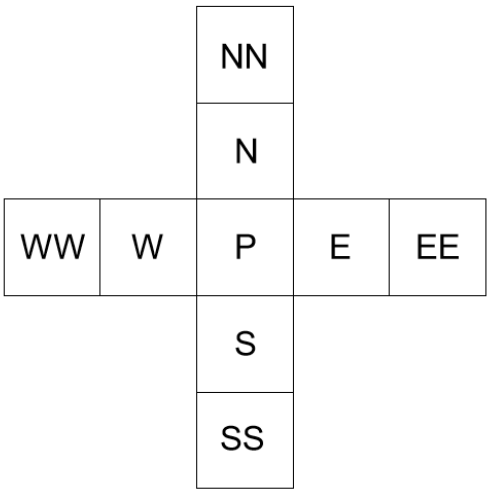

Figure 4.7: Second order molecule.

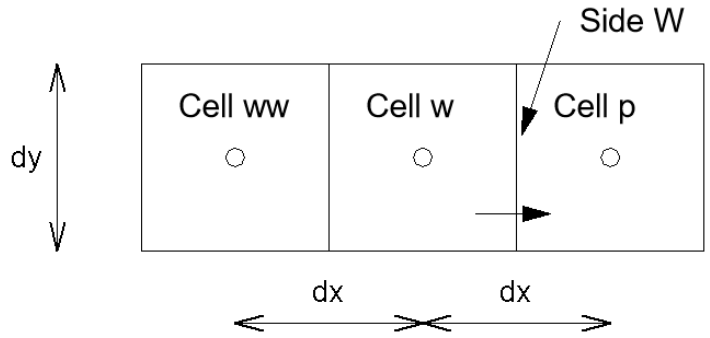

Figure 4.8: Estimation of quantity Φ at side W for cell p.

In figure 4.8 the principle for estimating quantity Φ using two upwind cells, w and ww, for the second order upwind scheme is shown. The quantities in cell w and ww are denoted Φ_w and Φ_{ww}, respectively, and are used to extrapolate linearly to side W. By triangulation, the expression of Φ on side W, denoted Φ^w, can be calculated (Olsen, 2017):

$$\Phi^w = \frac{3}{2}\Phi_w - \frac{1}{2}\Phi_{ww} \tag{14}$$

The flux through the sides of the molecule into cell p can be calculated as shown in the following equations (Olsen, 2017):

$$F_w = u_w A_w \left(\frac{3}{2}\Phi_w - \frac{1}{2}\Phi_{ww}\right) + \Gamma_w \frac{A_w(\Phi_w - \Phi_p)}{dx} \tag{15}$$

$$F_e = u_e A_e \left(\frac{3}{2}\Phi_p - \frac{1}{2}\Phi_w\right) + \Gamma_e \frac{A_e(\Phi_p - \Phi_e)}{dx} \tag{16}$$

$$F_s = u_s A_s \left(\frac{3}{2}\Phi_p - \frac{1}{2}\Phi_n\right) + \Gamma_s \frac{A_s(\Phi_p - \Phi_s)}{dy} \tag{17}$$

$$F_n = u_n A_n \left(\frac{3}{2}\Phi_n - \frac{1}{2}\Phi_{nn}\right) + \Gamma_n \frac{A_n(\Phi_n - \Phi_p)}{dy} \tag{18}$$

The resulting weighting factors of each cell can then be calculated by continuity and are shown in the following equations:

$$a_w = \frac{3}{2}u_w A_w + \Gamma_w \frac{A_w}{dx} + \frac{1}{2}u_e A_e \tag{19}$$

$$a_{ww} = -\frac{1}{2}u_w A_w \tag{20}$$

$$a_e = \Gamma_e \frac{A_e}{dx} \tag{21}$$

$$a_{ee} = 0 \tag{22}$$

$$a_n = \frac{3}{2}u_n A_n + \Gamma_n \frac{A_n}{dy} + \frac{1}{2}u_s A_s \tag{23}$$

$$a_{nn} = -\frac{1}{2}u_n A_n \tag{24}$$

$$a_s = \Gamma_s \frac{A_s}{dy} \tag{25}$$

$$a_{ss} = 0 \tag{26}$$

Equation (13) expressing the quantity Φ_p can for the Second Order Upwind scheme be rewritten as:

$$\Phi_p = \frac{a_w \Phi_w + a_e \Phi_e + a_n \Phi_n + a_s \Phi_s + a_{ww} \Phi_{ww} + a_{nn} \Phi_{nn}}{a_p} \tag{27}$$

The Second Order Upwind scheme provides more accurate results compared to the First Order Upwind scheme but does have some problems with oscillations and overshoots in some situations.

For the initial simulations both first and second order discretization schemes were tested. The second order scheme predicted high turbulent energy around the ribs, which would create suboptimal conditions for particles to settle. The First Order Upwind scheme predicted less turbulence around the ribs with quicker convergence. It was concluded that the first order scheme gave accurate results for the turbulent kinetic energy (Chirag Trivedi 2021, personal communication 23.03).

4.6.2 The SIMPLEC algorithm

The SIMPLE (Semi-Implicit Method for Pressure-Linked Equations) algorithm was first introduced by researchers Spalding and Patankar at the Imperial College in London (Patankar, 1980). The algorithm is used to find the unknown pressure field by guessing a pressure and finding an equation for a pressure-correction due to the continuity defect (Olsen, 2017). By adding the pressure-correction to the guessed pressure continuity is satisfied. The flow variables with the correction factors can be expressed as:

$$p = p^* + p' \tag{28}$$

$$u_k = u_k^* + u_k' \tag{29}$$

Where p and u are the pressure and velocity. The index k denotes the direction of the velocity, * is the initially calculated pressure that does not satisfy continuity, and ’ is the pressure correction. The discretized Navier-Stokes equation with guessed pressure values is expressed as (Olsen, 2017):

$$a_p u_{k,p^*} = \sum_{nb} a_{nb} u_{nb^*} + B_{u_k} - \left(A_k \frac{\partial p^*}{\partial \xi} \right) \tag{30}$$

Where a is the sum of the weighting factors, A_k is the surface area of the cell in direction k, and ξ is an index of the grid. B is a collection of the remaining terms from the discretization. The discretized version of the Navier-Stokes equation using corrected pressure values can be written as (Olsen, 2017):

$$a_p u_{k,p} = \sum_{nb} a_{nb} u_{nb} + B_{u_k} - \left(A_k \frac{\partial p}{\delta \xi} \right) \tag{31}$$

By subtracting equation 31 from equation 30, and implementing the correction equations 28 and 29, this equation can be written as (Olsen, 2017):

$$a_p u_{k,p}' = \sum_{nb} a_{nb} u_{k,nb}' - \left(A_k \frac{\partial p'}{\partial \xi} \right) \tag{32}$$

For the SIMPLE method, a simplification has been made to neglect the first term on the right-hand side of equation 32, and this gives the velocity correction equation:

$$u'_{k,p} = \frac{A_k \partial p'}{a_p \partial \xi} \tag{33}$$

In Ansys Fluent the SIMPLEC method is applied, which will be described in the following. The SIMPLEC algorithm uses a different formula for the velocity correction and has shown to converge earlier than the SIMPLE method (Olsen, 2017). The formula for the velocity correction factor applied in the SIMPLEC method is given in equation (34):

$$u'_{k,p} = \frac{A_k}{(a_p - \sum_{nb} a_{nb})} \frac{\partial p'}{\partial \xi} \tag{34}$$

From equation (34), the velocity-corrections are calculated once the pressure-corrections are known. The pressure-corrections are obtained by using the continuity equation for the velocity-corrections of a cell. Substituting the corrected values into the continuity equation leads to the equation for the pressure-correction (Olsen, 2017):

$$a_p p'_p = \sum_{nb} a_{nb} p'_{nb} + b \tag{35}$$

Where *b* is the deficiency from the incorrect velocity field u^*. The pressure correction obtained from equation (35), the correct pressure field can be calculated, and the continuity equation is satisfied. The iteration process can be summarized in the following procedure (Olsen, 2017):

1. Guess a pressure field, p^*.
2. Calculate the velocity $u^*$from equation (30).
3. Solve equation (35) to obtain the pressure-correction, p'.
4. Correct the pressure by adding $p'$to the guessed pressure p^*.
5. Correct the velocities u_k^* with u'_k using equation (34).
6. Repeat iteration from point 2 until convergence criterion is met.

4.6.3 Turbulence modelling

The flow of a fluid can be categorized as either laminar, transitional or turbulent. Laminar flow is characterized by steady, parallel streamlines, and typically only occurs at low velocities. Turbulent flow is associated with higher velocities and is characterized by velocity fluctuations and chaotic flow patterns. In the transitional zone the flow fluctuates between laminar and turbulent over a region before it becomes fully turbulent (Çengel & Cimbala, 2010). Figure 4.9 shows the three different flow categories:

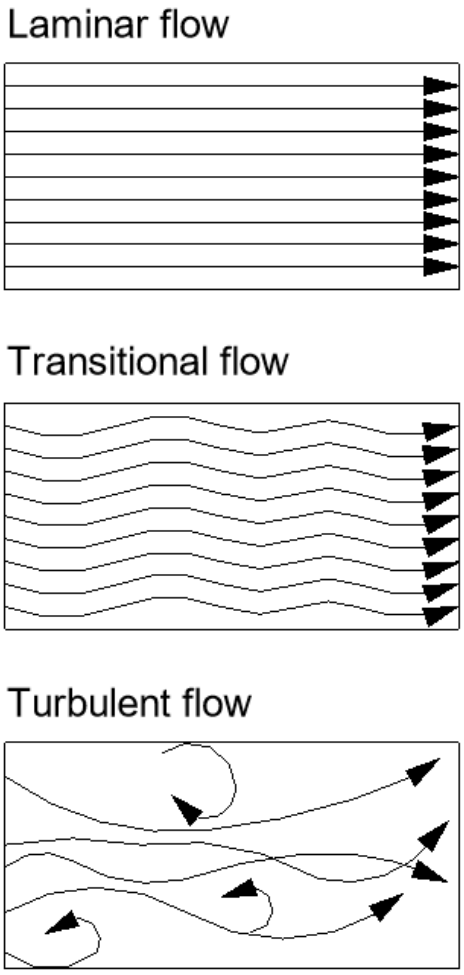

Figure 4.9: Laminar, transitional, and turbulent flow.

In the 1880s, Osborne Reynolds performed experiments investigating how different parameters affected the flow of a fluid, and found that the flow regime mainly depends on the ratio of inertial to viscous forces (Çengel & Cimbala, 2010):

$$Re = \frac{Inertial\ forces}{Viscous\ forces} = \frac{ud}{\nu} = \frac{\rho u d}{\mu} \tag{36}$$

Where *Re* is the dimensionless Reynolds number [-], u is the flow velocity [m/s], d is the diameter [m], ν is the kinematic viscosity of water [m^2/s], ρ is the water density [kg/m^3], and μ is the dynamic viscosity of water [Ns/m^2]. If the inertial forces are dominating, equation (36) results in a high Reynolds number and turbulent flow. If the viscous forces are dominating, the flow is associated with a low Reynolds number, and is considered laminar. In table 1 an overview of the different flow regimes is shown (Çengel & Cimbala, 2010):

Table 1: Flow type as a function of Reynolds number.

Flow type	Reynolds number
Laminar flow	Re ≤ 2300
Transitional flow	2300 ≤ Re ≤ 4000
Turbulent flow	Re ≥ 4000

There exist several different methods to simulate turbulence in CFD modelling. The choice of model depends on the required accuracy of the model, and the available time and computational resources. The method of Direct Numerical Simulations (DNS) compute all the turbulent velocity fluctuations and can provide an accurate description of the turbulent flow. Unsteady Navier-Stokes equations are solved on fine grids with time steps small enough to compute all fluctuations, which is very computationally demanding (Versteeg & Malalasekera, 2007). Large Eddy Simulation (LES) is a turbulence model that differentiates between large and small eddies when calculating the flow. The method uses a spatial filtering of the unsteady Navier-Stokes equations that ignores eddies under a certain threshold (Versteeg & Malalasekera, 2007). The effect of the smaller eddies is included in the main flow with a sub-grid scale model. LES modelling is less computationally demanding than DNS, but still requires a lot of resources due to the computation of unsteady flow equations.

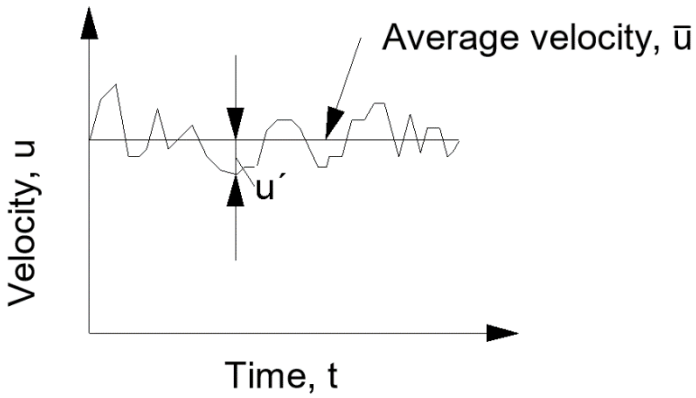

Figure 4.10: Time averaging of velocity.

The third method to simulate turbulence is the Reynolds-Averaged Navier-Stokes equations (RANS). The turbulence is not solved directly as for LES and DNS, but time averaged Navier-Stokes equations are calculated before applying numerical methods to observe the effect of turbulence on the mean flow (Versteeg & Malalasekera, 2007). Figure 4.10 shows how the velocity is time averaged, and this results in the following expression for the velocity $u = \bar{u} + u'$, where u' is the fluctuating velocity. The same method is applied for the time averaged pressure. The time averaged Navier-Stokes equations can be expressed as:

$$\rho\frac{\partial\overline{u}_i}{\partial t}+\rho\frac{\partial\overline{u}_i\overline{u}_j}{\partial x_j}=-\frac{\partial\overline{p}}{\partial x_i}+\mu_t\frac{\partial^2\overline{u}_i}{\partial x_j^2}-\frac{\partial}{\partial x_j}(\rho\overline{u_i^{\prime}\,u_j^{\prime}}) \tag{37}$$

The velocity fluctuations from the time averaged values result in an extra term in the RANS equations called the Reynolds stress term, and describes extra stresses caused by turbulence (Versteeg & Malalasekera, 2007). The Reynolds stress terms are modelled with turbulence models such as the *k*-ε, *k*-ω, and the Reynolds stress model. The turbulence models are computed using the Boussinesq relationship shown in equation (38). The RANS method of simulating turbulence is less computationally demanding than the LES and the DNS methods, and is therefore commonly used for engineering purposes.

$$-\left(\rho\overline{u_i^{\prime}\,u_j^{\prime}}\right)=\mu_t\left(\frac{\partial U_i}{\partial x_j}+\frac{\partial U_j}{\partial x_i}\right)-\frac{2}{3}\rho k\delta_{ij}=2\mu_t S_{ij}-\frac{2}{3}\rho k\delta_{ij} \tag{38}$$

Where μ_t is the eddy viscosity [m^2/s], *k* is the turbulent kinetic energy [m^2/s^2] and δ_{ij} is the Kronecker delta, which is 1 if i=j and 0 otherwise (Olsen, 2017). In equation (39) the rate of deformation of a fluid element, S_{ij}, is expressed (Versteeg & Malalasekera, 2007):

$$S_{ij}=\begin{bmatrix}S_{xx} & S_{xy} & S_{xz}\\ S_{yx} & S_{yy} & S_{yz}\\ S_{zx} & S_{zy} & S_{zz}\end{bmatrix} \tag{39}$$

For this master thesis the shear-stress transport (SST) *k*-ω turbulence model will be used. The SST *k*-ω is a hybrid turbulence model proposed by Florian R. Menter in 1992, using a standard *k*-ε turbulence model converted to a *k*-ω formulation in the fully turbulent region that transforms into a *k*-ω in the near-wall region (Versteeg & Malalasekera, 2007). The transformed *k*-ε and the *k*-ω are multiplied with a blending function that is 1 in the near-wall region, activating the *k*-ω model, and 0 away from the wall, which activates the transformed *k*-ε function (Ansys Fluent).

For the *k*-ε model two transport equations are solved, one for *k and one for* ε, to define the velocity and length scale of the turbulence. The kinematic eddy viscosity ν_t[m^2/s] is expressed as a product of a turbulent velocity scale $v=\sqrt{k}$ and a length scale $\ell=k^{3/2}/\varepsilon$ where *k* is the turbulent kinetic energy and ε is the rate of dissipation of kinetic energy (Versteeg & Malalasekera, 2007). To transform the *k*-ε model to a *k*-ω model, the second equation is solved for the turbulence frequency $\omega=\varepsilon/k$ [s^{-1}] instead of the dissipation rate ε resulting in a length scale $\ell=\sqrt{k}/\omega$. The eddy viscosity is given as (Versteeg & Malalasekera, 2007):

$$\mu_t=\rho k/\omega \tag{40}$$

The Reynolds stresses are computed with the Boussinesq expression from equation (38), and the transport equation for the turbulent kinetic energy *k* is expressed as (Versteeg & Malalasekera, 2007):

$$\frac{\partial(\rho k)}{\partial t} + div(\rho k U) = div\left[\left(\mu + \frac{\mu_t}{\sigma_k}\right) grad(k)\right] + P_k - \beta^* \rho k \omega \tag{41}$$

$$P_k = \left(2\mu_t S_{ij} \,.\, S_{ij} - \frac{2}{3}\rho k \frac{\partial U_i}{\partial x_j}\delta_{ij}\right) \tag{42}$$

Where P_k is the rate of production of turbulent kinetic energy and the transformed ε equation for ω results in (Versteeg & Malalasekera, 2007):

$$\begin{aligned}\frac{\partial(\rho\omega)}{\partial t} + div(\rho\omega U) = \; & div\left[\left(\mu + \frac{\mu_t}{\sigma_{\omega,1}}\right) grad(\omega)\right] + \\ & \gamma_2\left(2\rho S_{ij} \,.\, S_{ij} - \frac{2}{3}\rho\omega\frac{\partial U_i}{\partial x_j}\delta_{ij}\right) - \beta_2\rho\omega^2 + 2\frac{\rho}{\sigma_{\omega,2}}\frac{\partial k}{\partial x_k}\frac{\partial \omega}{\partial x_k}\end{aligned} \tag{43}$$

The constants used in the SST *k*-ω are based on experience of the model to optimize the performance compared to the original *k*-ω turbulence model (Versteeg & Malalasekera, 2007). A summary of the improved constant values is presented in table 2 (Menter et al., 2003):

Table 2: Model constants in the SST *k*-ω turbulence model.

σ_k	1.0
$\sigma_{\omega,1}$	2.0
$\sigma_{\omega,2}$	1.17
γ_2	0.44
β_2	0.083
β^*	0.09

4.6.4 Errors and uncertainty in CFD

Numerical simulation with CFD can provide cost efficient and quick results for a wide range of engineering problems. However, the consequences of relying on CFD simulations of low quality can be costly, or even more severe, depending on its use. The following definitions of error and uncertainty in CFD modelling are widely accepted (AIAA, 1998):

- *Error: a recognizable deficiency in a CFD model that is not caused by lack of knowledge.*
- *Uncertainty: a potential deficiency in a CFD model that is caused by lack of knowledge.*

A summary of the errors and uncertainties is presented in table 3 (Versteeg & Malalasekera, 2007):

Table 3: Summary of errors and uncertainty in CFD.

Numerical errors	
Roundoff error	The number of significant digits may affect the solution accuracy.
Iterative convergence error	The difference between the converged solution and the solution after *i* iterations.
Discretization error	Neglecting contributions from higher order discretization schemes may affect the solution.
Coding errors	Bugs in the software.
User errors	Incorrect use of CFD program.
Input uncertainty	
Domain geometry	Difference in intended geometry and the geometry applied in the CFD model.
Boundary conditions	The type and location of boundary conditions, together with simplified assumptions affect the solution.
Fluid properties	Inaccurate assumption of constant fluid properties e.g., density and viscosity.
Physical model uncertainty	
Limited accuracy or lack of validity of submodels.	Simulating complex flow phenomena, such as turbulence using semi-empirical submodels.
Limited accuracy or lack of validity of simplifying assumptions.	The accuracy of simplifying assumptions contributes to physical model uncertainty.

4.7 Simulation setup for calibration and validation

This section presents the simulation plan for the validation of the numerical model and preparing the model for the simulations used to test the hypotheses.

1. Steady state SST k-ω RANS simulations are run with two different discharges to calibrate and validate the CFD model with data from the PIV experiments.
2. Transient SST k-ω RANS simulations with sediments are run to find a particle diameter that results in a trap efficiency of 50%.

4.7.1 Calibration and validation

The simulations are performed using Ansys Fluent with the double precision solver. The double precision option is chosen to include more decimals in the calculations, thus increasing the accuracy as described in section 4.6.4. The fluid *water-liquid (h20<>l)* is selected as the fluid material, as opposed to the default fluid air.

The turbulence is modelled with the SST *k-*ω turbulence model. For the pressure-velocity coupling the SIMPLEC discretization is used. The First Order Upwind scheme is applied to the equations of momentum, the turbulent kinetic energy, and specific dissipation rate. The convergence criterion is set to 1e-06. $Q_p = L_R{}^{\frac{5}{2}} Q_m$

To simulate the different surfaces in the model, roughness height and constants must be applied for the walls, bed, and ribs. The roughness height is a measure of the surface friction, where a value of 0 would imply a smooth surface. In Ansys Fluent the roughness height is given in meters, and the roughness constant has a value between 0 and 1. The bed and ribs are assumed to be concrete lined, resulting in the same roughness values. The walls are simulated as unlined rock, resulting in a higher roughness height compared to the concrete lined surfaces. Table 4 summarizes the values assigned to the different surfaces (Kaspar Vereide 2021, personal communication, 12.03).

Table 4: Roughness height and roughness constant.

	Roughness height [m]	Roughness constant [-]
Walls	0.30	1.00
Bed & ribs	0.02	0.50

The boundary conditions for the walls are defined by a no-slip condition, where the velocity at the walls is zero. The CFD model is calibrated and validated through comparison with results from the PIV experiments in the hydraulic laboratory. PIV experiments with seven different discharges were conducted in the physical model, to investigate how the ribs separated the flow as a function of discharge. For comparison with the physical model, CFD simulations are run with model discharges, Q_m of 40 l/s and 100 l/s. The inlet velocities for the CFD simulations are calculated from the relationship from Froude's scaling law equation (44, 45 and 46) (Guttormsen, 2013):

$$L_R = \frac{L_p}{L_m} \tag{44}$$

Where L_R [-] is the dimensionless length scale, L_p [m] is the prototype length and L_m [m] is the model length.

$$u_p = \sqrt{L_R}\, u_m \tag{45}$$

Where u_p [m/s] is the water velocity in the prototype and u_m [m/s] is the water velocity in the model.

$$Q_p = L_R^{\frac{5}{2}} Q_m \tag{46}$$

Where Q_p [m^3/s] is the prototype discharge and Q_m [m^3/s] is the model discharge. The physical model was built in a scale of 1:20, meaning the length scale from equation (44) is $L_R = 20$. The inlet velocity can then be calculated by continuity, shown for the case relating to the 40 l/s model discharge in equation (47):

$$u_{in} = \frac{Q}{A_{in}} = \frac{71.6\ \frac{m^3}{s}}{\left(5\ m\ \cdot 11\ m + \frac{\pi \cdot 5.5\ m^{\,2}}{2}\right)} = 0.70\ \frac{m}{s} \tag{47}$$

Where A_{in} is the cross-sectional area of inlet section of the CFD model. A summary of the calculations is shown in table 5.

Table 5: Inlet velocity for validation of CFD model.

Model discharge (Q_m)	Prototype discharge (Q_p)	Inlet velocity (u_{in})
0.04 m^3/s	71.6 m^3/s	0.70 m/s
0.1 m^3/s	178.9 m^3/s	1.76 m/s

An overview of the numerical methods and applications used for the calibration and validation of the CFD model is shown in table 6.

Table 6: Summary of numerical approach.

Numerical method	
Solver	Pressure-based
Pressure-velocity coupling	SIMPLEC
Discretization	
Convective equations	First Order Upwind
Gradient	Least Square Cell based
Boundary conditions	
Inlet	Velocity inlet, $u_{in,1} = 0.70\frac{m}{s}, u_{in,2} = 1.76\frac{m}{s}$
Outlet	Pressure outlet, p = 0 Pa
Walls	No-slip

The results from the PIV experiments are given as vector plots and line charts showing the average horizontal velocity as a function of the vertical position from the model bed to 100 mm above the top of the rib. In figure 4.11 the vector and line chart of the setup for the PIV experiments for the 40 l/s case is shown (Havrevoll et al., 2021).

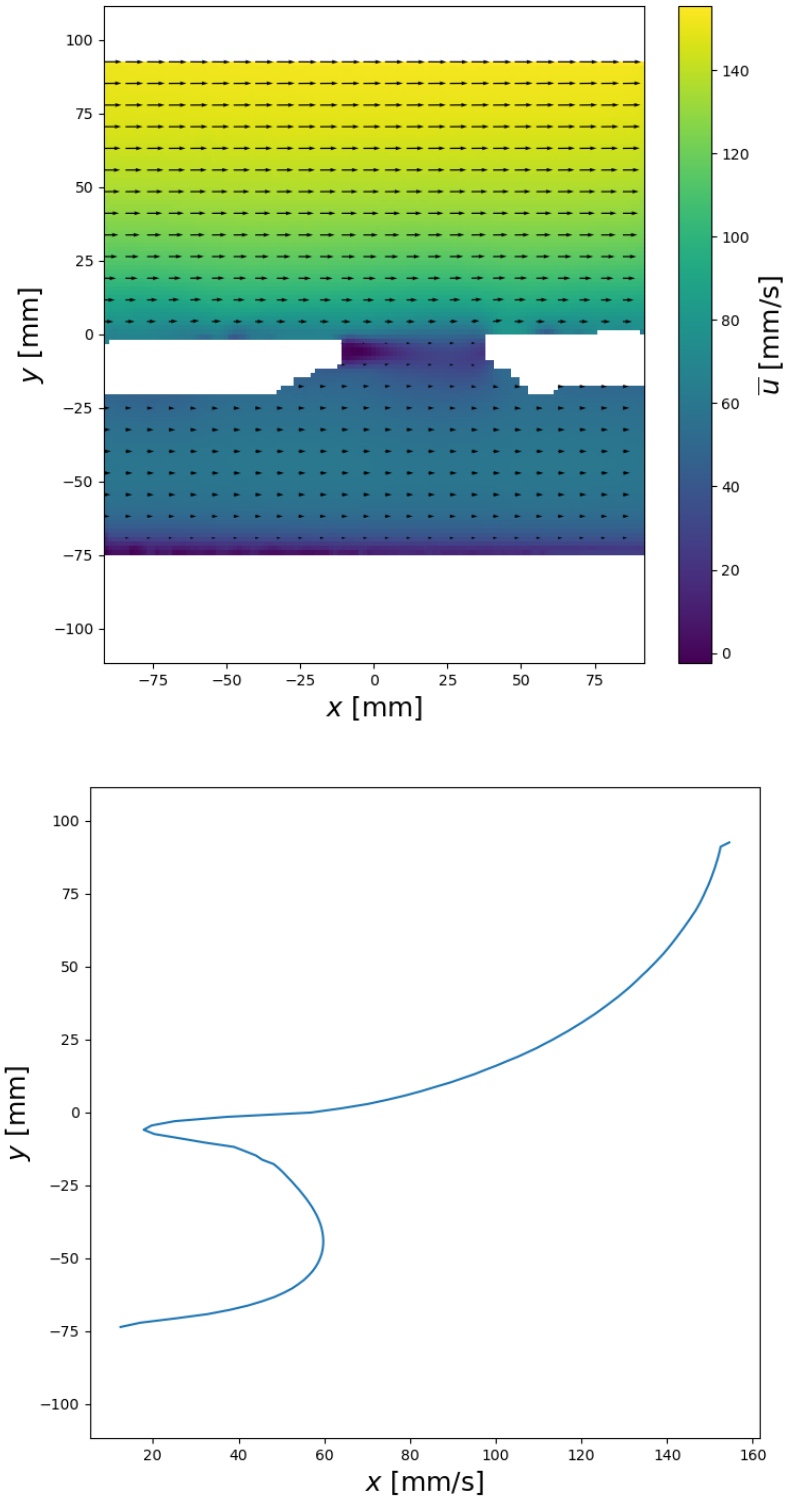

Figure 4.11: Horizontal velocity for the 40 l/s case presented with a vector plot and a line chart with values in model scale.

From figure 4.11 the view of the PIV camera is shown, where the mid-point is between the ribs. The camera is placed downstream of the access tunnel, a short distance upstream the weir. To compare the simulation results to the PIV experiments, a surface is inserted in the CFD model at position x = 169.5 m, between two ribs, to be used as a control section. The placement of the control section is chosen to be comparable to the placement of the camera in the physical model. The vertical position y in figure 4.11 is transformed to prototype scale using equation (44), to obtain vertical control sections for comparison with the CFD model. The horizontal velocities x, from the PIV results are read graphically from the figures for both the 40 l/s and the 100 l/s case and transformed to prototype scale using equation (45).

In the post-processing of the CFD results, five points are inserted at the control section. The horizontal velocity is calculated at the symmetry plane corresponding to the middle of the model at five different vertical positions as shown in table 7:

Table 7: Corresponding vertical position from physical model to CFD model.

Vertical position physical model [mm]	Vertical position CFD model [m]
-50	-1.0
-25	-0.5
0 (top of rib)	0 (top of rib)
25	0.5
50	1.0
75	1.5

The comparisons of the horizontal velocity between the physical model and the CFD simulations are shown for both discharges in figure 4.12. The velocity above the ribs has a good fit between the measured and the simulated values for both discharges, being slightly higher for the 71.6 m^3/s case. The velocity under the ribs is simulated to be slightly higher than the measured values from the physical model. The measured field in the PIV experiment is limited to 1.5 m above the rib in prototype scale, meaning that there is 6 m up to the roof of the model that is not included in the view. Based on the CFD models accuracy compared to the physical model, and the discharge used for further simulations lying in between the two calibration discharges at 85 m^3/s, it was concluded that the validation was satisfactory to proceed with experiments (Kaspar Vereide, 2021, personal communication 23.04).

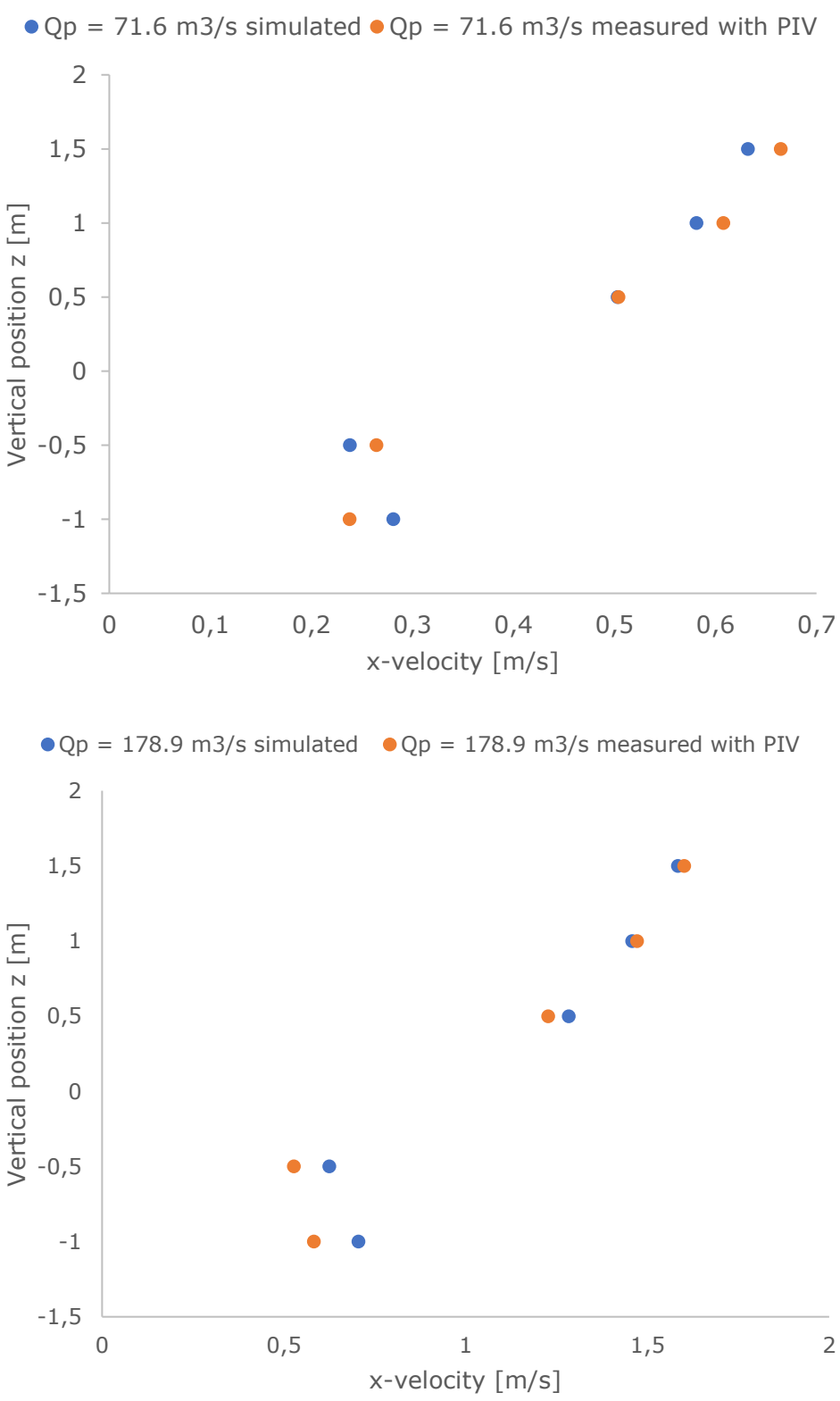

Figure 4.12: Calibration between PIV experiments and CFD model shown in prototype scale.

4.7.2 Selection of particle diameter

To compare the different rib designs, and how they affect the flow, transient simulations with sediments are run to find a particle diameter that results in a trap efficiency of roughly 50%. An injection is created after activating the Discrete Phase Model (DPM) in Ansys Fluent. The particles are injected from a surface 5 m downstream of the velocity inlet, evenly distributed over the surface. The sediment inlet can be seen in figure 4.13.

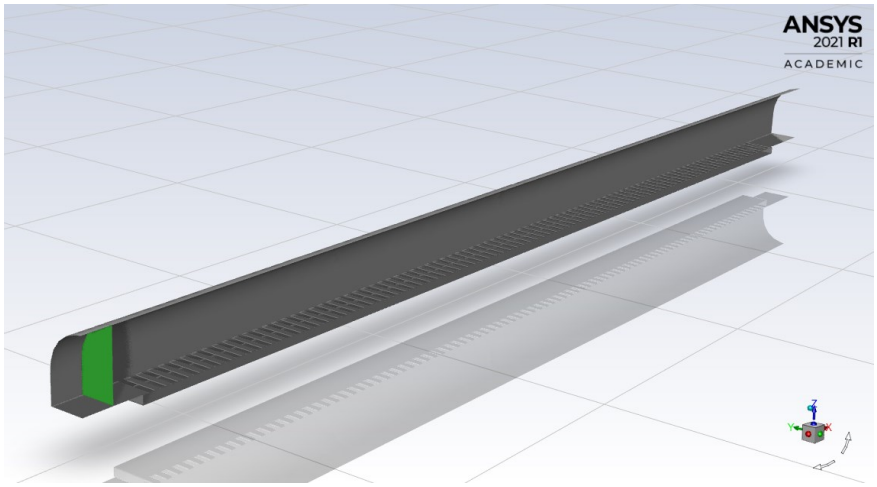

Figure 4.13: Sediment inlet

The numerical setup and boundary conditions are kept the same for the transient simulations as for the steady-state simulations, except the inlet velocity. It is planned to upgrade turbine no. 5 in Tonstad from 80 m^3/s to 85 m^3/s during an upcoming turbine rehabilitation project (Kaspar Vereide 2021, personal communication 12.03). The inlet velocity is calculated using equation (37) with a discharge of 85 m^3/s, resulting in an inlet velocity of 0.83 m/s.

Three different sediment diameters are injected to test the trap efficiency. For the first simulation particles with diameter 0.3 mm are injected to compare the trap efficiency to the simulation of sandtrap no. 3 by Næss (2020). The simulation is run until all the sediments are either trapped or escaped, resulting in a flow time of 300 seconds. For the second and third simulations sediments with a diameter 0.2 mm and 0.1 mm are injected. The simulations were run for 400 seconds and 515 seconds, respectively. The momentum convergence plots for the simulations with particles with diameter 0.3 mm and 0.1 mm are shown in figure 4.14. To track the sediment trajectories in the simulation, *Particle Tracks* is turned on before running the calculations. This creates a plot showing the particle trajectories, colored by the particle residence time. When the calculation is finished, a summary of the particles is printed to the Fluent console, showing the number of sediments released, trapped and escaped. The trap efficiencies can then be calculated using equation (8), and the results are shown in table 8.

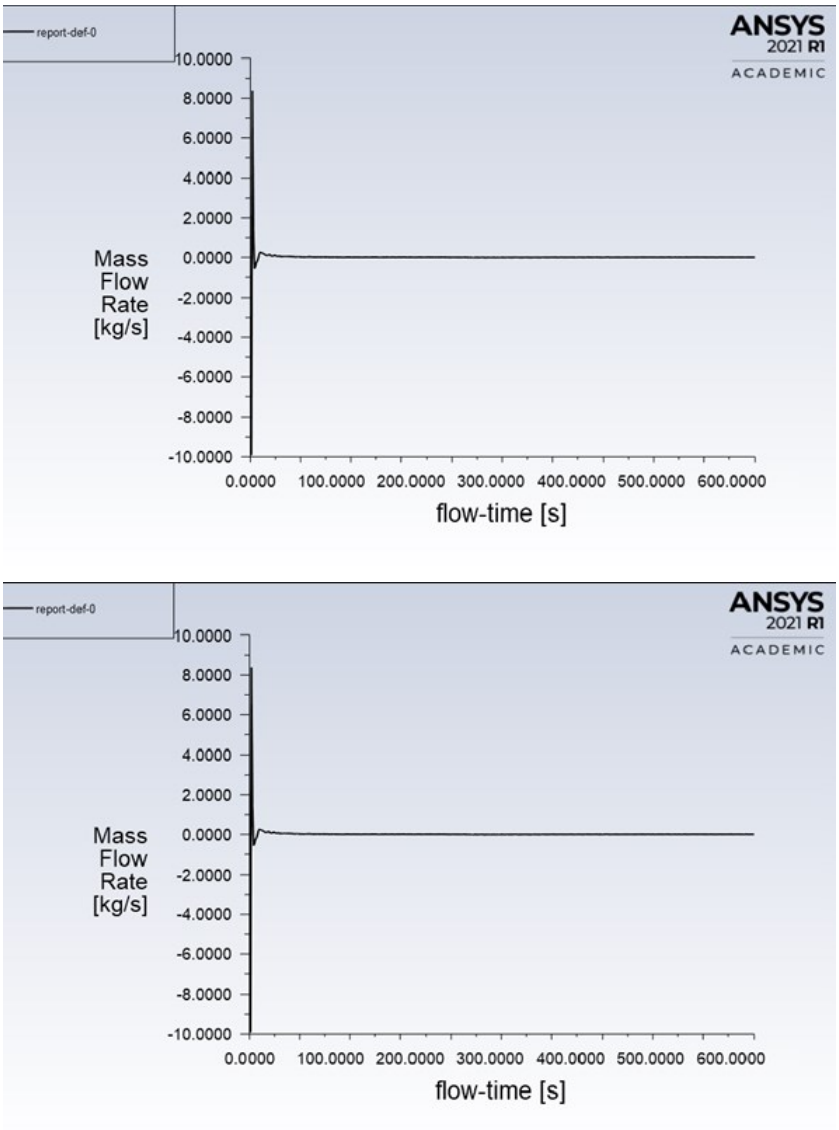

Figure 4.14: Mass flow rate convergence for the 0.3 mm and 0.1 mm simulations, respectively.

Table 8: Trap efficiency.

Particle diameter	Trap efficiency
0.3 mm	94.4%
0.2 mm	73.8%
0.1 mm	44.2%

The injection of particles with a diameter of 0.3 mm resulted in a trap efficiency of 94.4%, compared to 93.4% for sandtrap no. 3 rebuilt with ribs (Næss, 2020). It is pointed out the two models are not exactly similar and a small discrepancy was expected. A summary of the sediment injection is shown in table 9:

Table 9: Sediment injection setup.

Inlet velocity	0.83 m/s
Injection type	Surface
Particle type	Inert
Diameter distribution	Uniform
Particle density	2650 kg/m^3
X, Y, Z velocity	0 m/s
Start time	0 s
Stop time	20 s
Total flow rate	1 kg/s
Time step	1 s
Iterations per time step	20

In addition to the boundary conditions applied for the steady-state simulations, there are several boundary conditions applied for the discrete phase. The boundary condition for the inlet and the outlet is *escaped*, where the particles disappear if they meet the boundary. The boundary conditions for the walls and the ribs are set to *reflect*. The normal and tangential coefficient of restitution is set to 0.9 based on experience (Wolfgang Richter & Kaspar Vereide 2021, personal communication 14.04). The boundary condition for the bed is set to *trapped*, meaning that calculations are ended for particles hitting the bed of the sandtrap.

4.8 Simulation setup for testing the hypotheses

This section presents the numerical setup for the different simulations for the two hypotheses. The simulations are run with the same numerical methods as in section 4.7.2 and with 0.1 mm particles. The rib design is changed for each simulation using SpaceClaim. Minor adjustments are made to the length of the rib section to make sure the first and last rib are full width. A new meshing process must also be carried out for every rib design. To observe the effect of the rib design on the trap efficiency, 10 simulations are run for each hypothesis, 5 larger and 5 smaller than the 1x1 meter initial simulation. An overview of the different rib designs are shown in table 10.

Table 10: Summary of the different rib designs used in the simulations.

Simulation setup when rib width is equal to the opening between the ribs.		
Simulation #	Rib width [m]	Opening [m]
1*	0.30	0.30
2	0.40	0.40
3	0.50	0.50
4	0.60	0.60
5	0.75	0.75
6	1.00	1.00
7	2.00	2.00
8	3.00	3.00
9	4.00	4.00
10	5.00	5.00
Simulation setup when rib width is 1 meter, and the rib opening varies.		
11	1.00	0.30
12	1.00	0.40
13	1.00	0.50
14	1.00	0.60
15	1.00	0.75
16	1.00	1.00
17	1.00	2.00
18	1.00	3.00
19	1.00	4.00
20	1.00	5.00

* For simulation 1, the rib section was shortened to 60 m compared to 180 m for the other simulations to cope with the limitation of 512 000 elements in the academic version of Ansys Fluent. This rib design was not close to the optimum and this difference compared to the other simulations is therefore not important to the conclusions.

4.9 Summary of verification tests for the numerical methods

This section will present a summary of the verification tests that led to the basis of the numerical methods used in this thesis. The summary is presented in table 11.

Table 11: Summary of verifications for the numerical methods

Discretization scheme	The initial plan was to use Second Order Upwind schemes for the discretization, as it is regarded as more accurate than First Order Upwind schemes. Both first and second order schemes were tested. Based on recommendations from Chirag Trivedi (personal communication, 23.03.21), the first order scheme was chosen as it provided the most accurate results.
Longer inlet	To investigate the effect of a longer inlet section, steady flow simulations were performed for two cases: 1) where the inlet was 77 m long, and 2) where the inlet was 10 m long. The effects of the longer inlet were small, and it was concluded to keep the short inlet to improve the grid resolution.
Mesh	Prior to running the initial simulations with sediments, Chirag Trivedi (personal communication, 29.04.21), provided recommendations to the meshing process regarding boundary layers and grid resolution. These recommendations formed a basis for the following simulations. After all the simulations were finished, Chirag Trivedi (personal communication, 25.05.21), assisted with an additional check of the meshes and the validity of the results.
Numerical setup	Wolfgang Richter (personal communication, 14.04.21) gave recommendations to the numerical setup regarding coefficient of restitution, roughness heights and coefficients and general method.
Post simulation check	Before analyzing the results, a check of the simulation setup was performed for all the simulations. This was done to make sure that all the simulations were performed with the exact same numerical setup. And that the simulations on the two different computers with the same setup did not give different results.

5 Results

5.1 Reference case: 1m by 1 m rib setup

In this section, several figures showing the flow situation for the rib setup of 1 m width and 1 m opening are presented to provide a basis for the particle movement through the sandtrap. An overview plot showing the turbulent kinetic energy along the symmetry plane and the bed is given in figure 5.1, respectively.

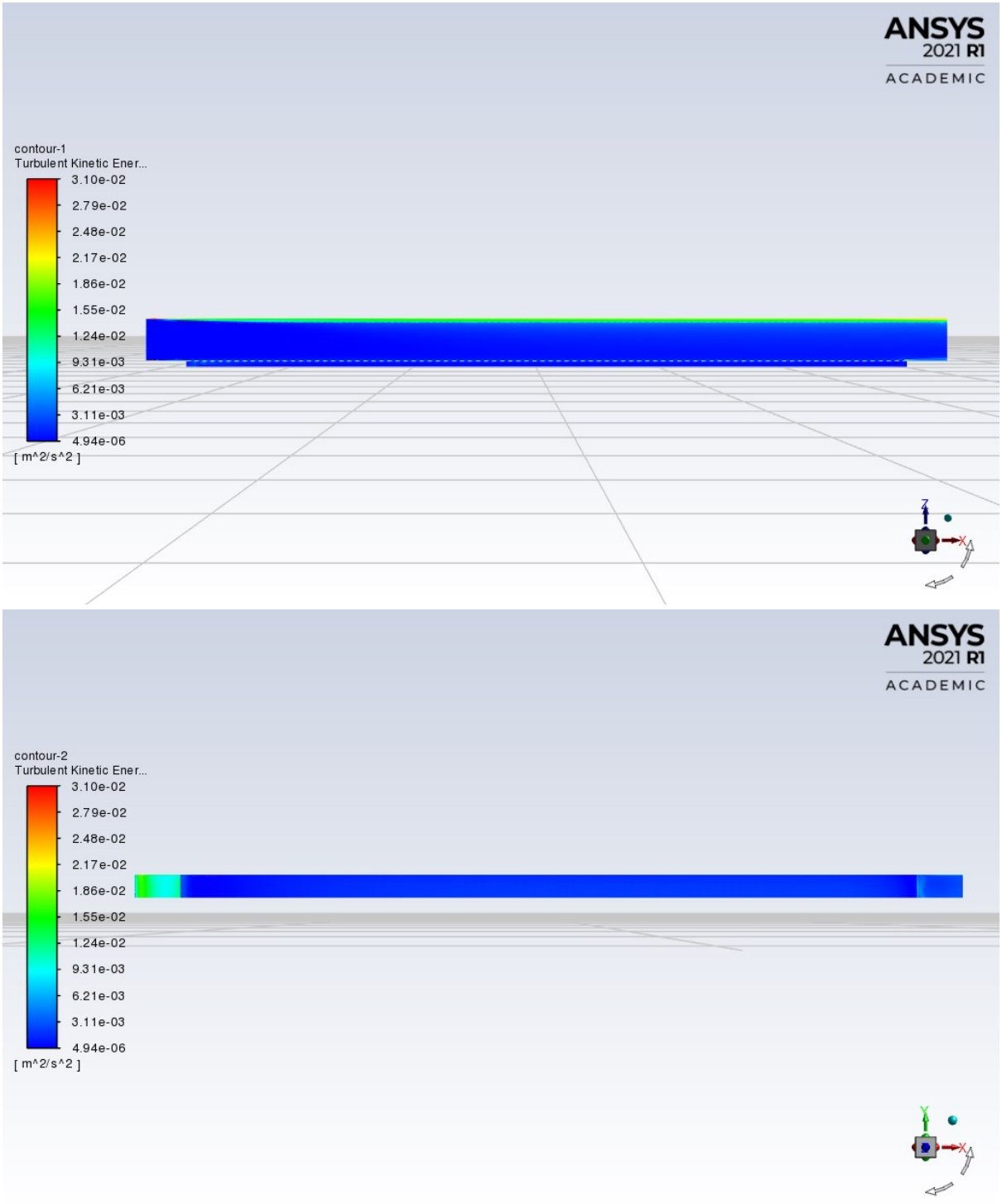

Figure 5.1: Turbulent kinetic energy along the symmetry plane and the bed.

A detailed plot showing the kinetic turbulent energy along the symmetry plane for the inlet and outlet section is given in figure 5.2, respectively. Higher turbulence can be observed along the roof of the model, in addition to increased turbulence for the first few ribs. The turbulent kinetic energy is also higher for the last couple of ribs and along the bed in the outlet section.

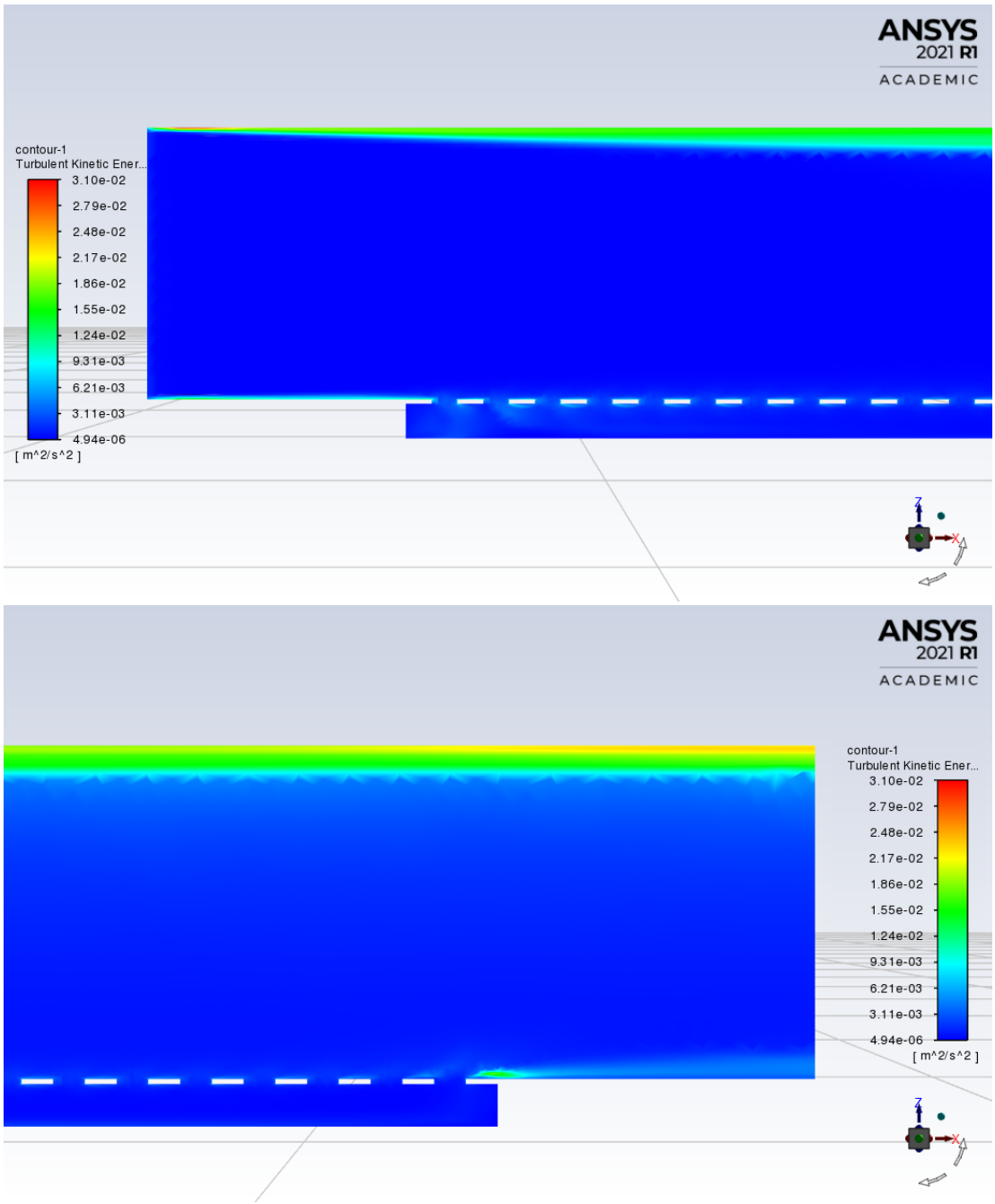

Figure 5.2: Detailed view of kinetic energy for the inlet and outlet sections.

In figure 5.3, a detailed vector plot of the velocity along the symmetry plane is given. The effect of the ribs separating the main flow from the storage volume can be seen, with lower velocities under the ribs. A circulation zone under the first and the last rib is observed, which may affect the sedimentation of particles and will be discussed in later sections.

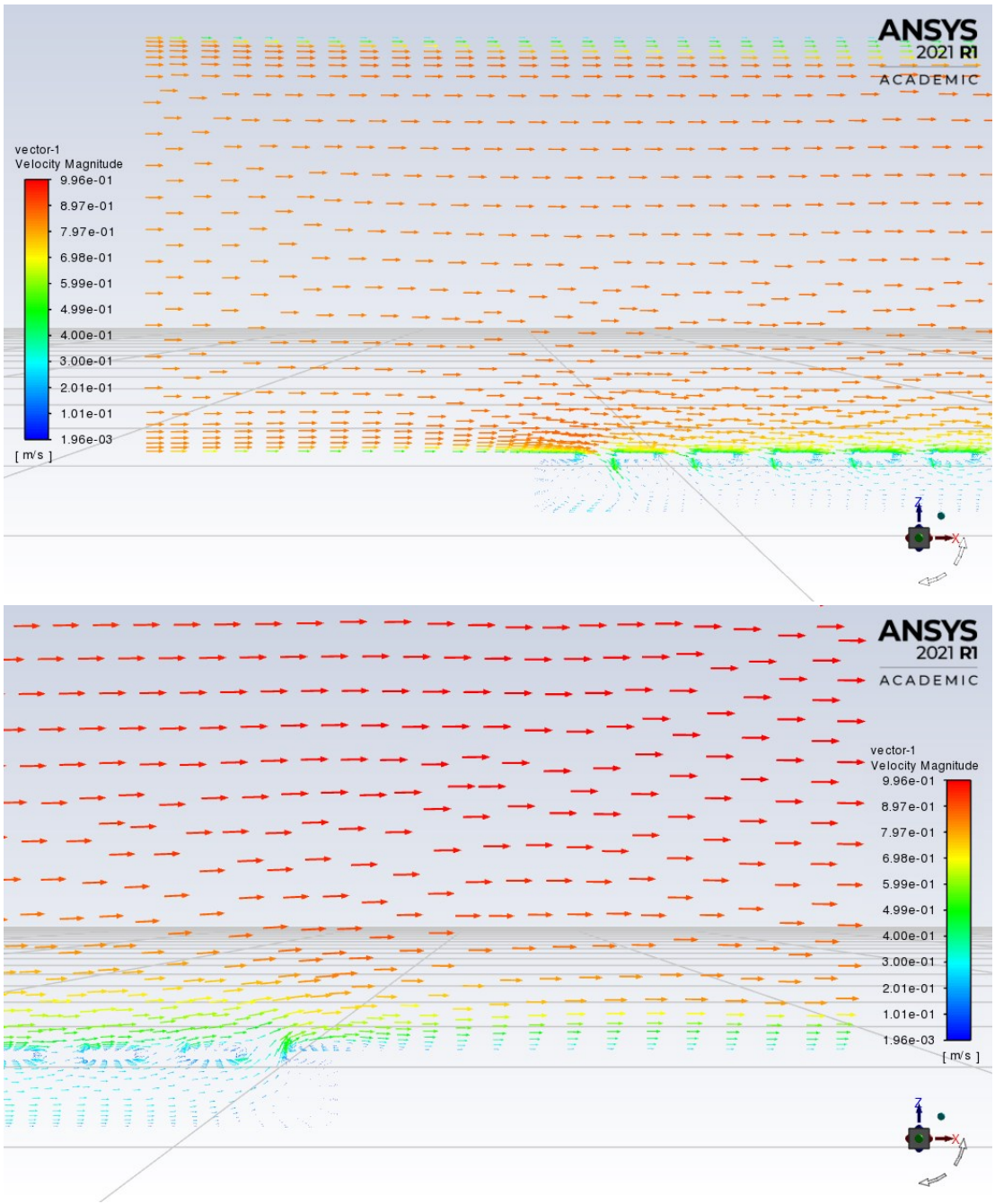

Figure 5.3: Detailed vector plot of the velocity along the symmetry plane for the inlet and outlet.

Figure 5.4 – 5.6 shows the particle trajectories as a function of the particle residence time for the 0.1 mm injection for the rib setup with 1 m wide ribs and 1 m opening. The movement of the particles through the model can be seen at different timesteps of the simulation.

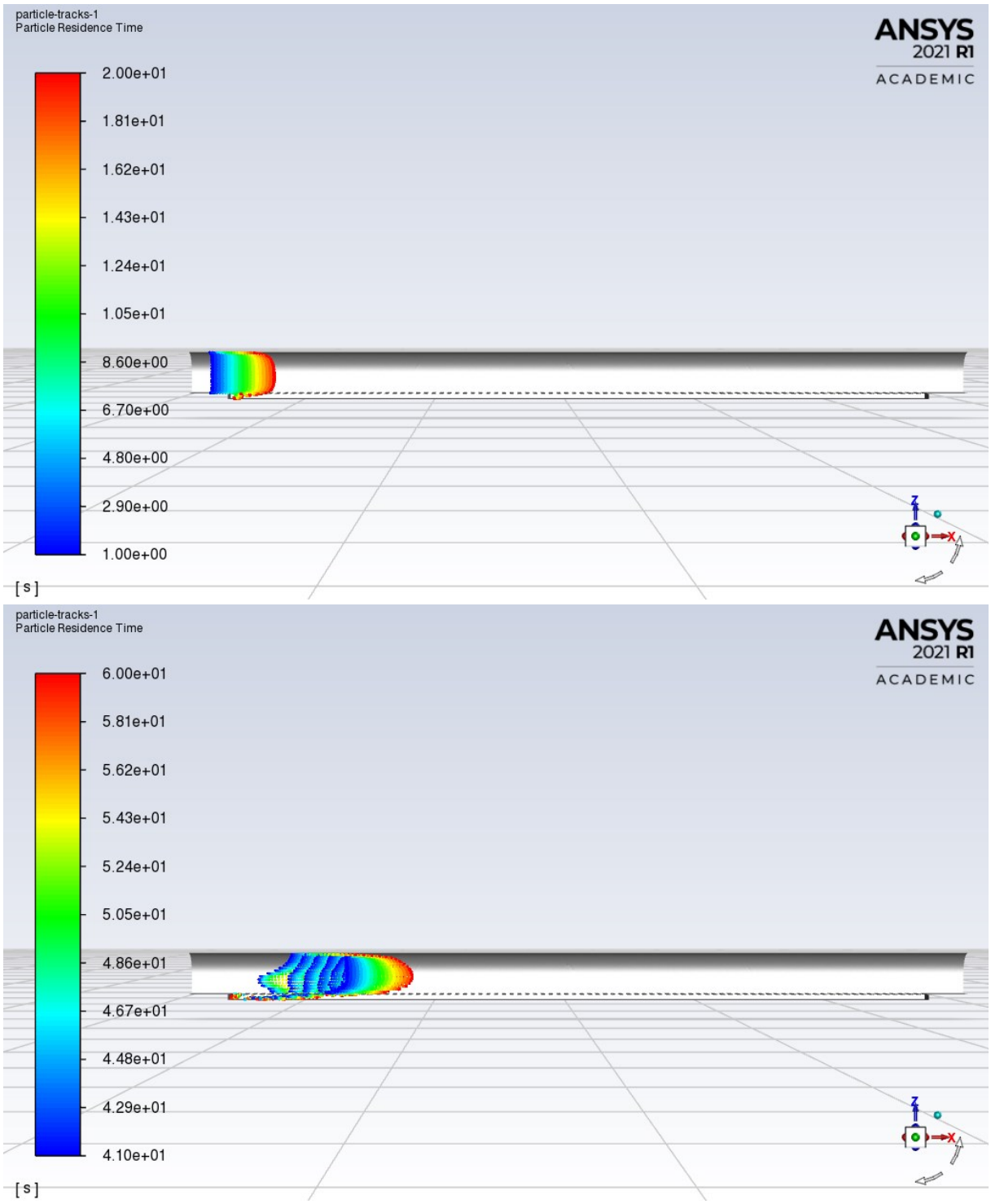

Figure 5.4: Injection of 0.1 mm particles after 60 s and 120 s.

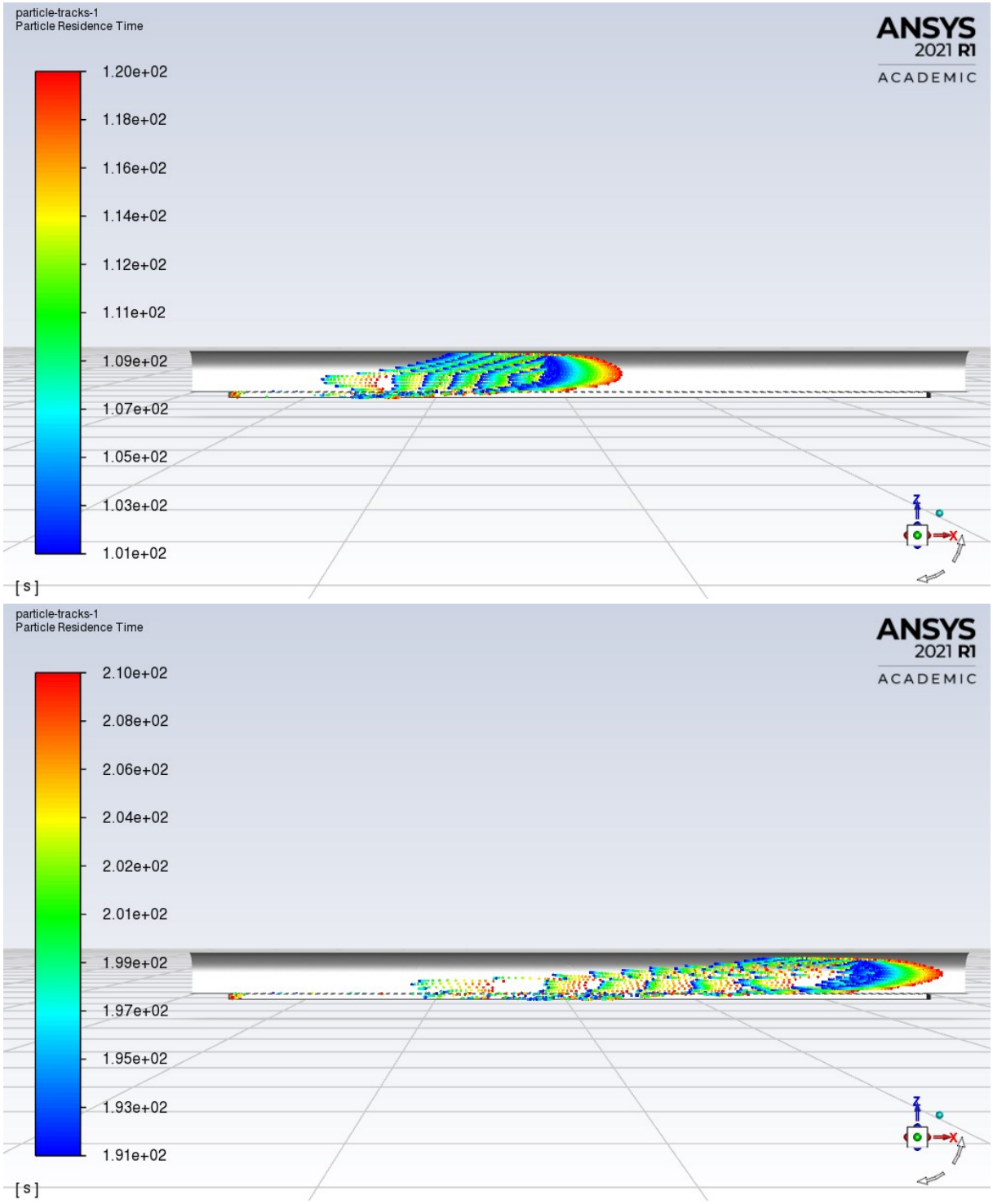

Figure 5.5: Injection of 0.1 mm particles at 120 s and 210 s

The effect of the recirculation zones at the first and last rib can be seen at the timestep 350 s in figure 5.6. A detailed plot of the particle trajectories shows that particles are kept in suspension in the recirculation zone under the first rib. For the last rib, the recirculation zone results in a backflow that leads some particles away from the bed up between the ribs, allowing them to escape through the outlet.

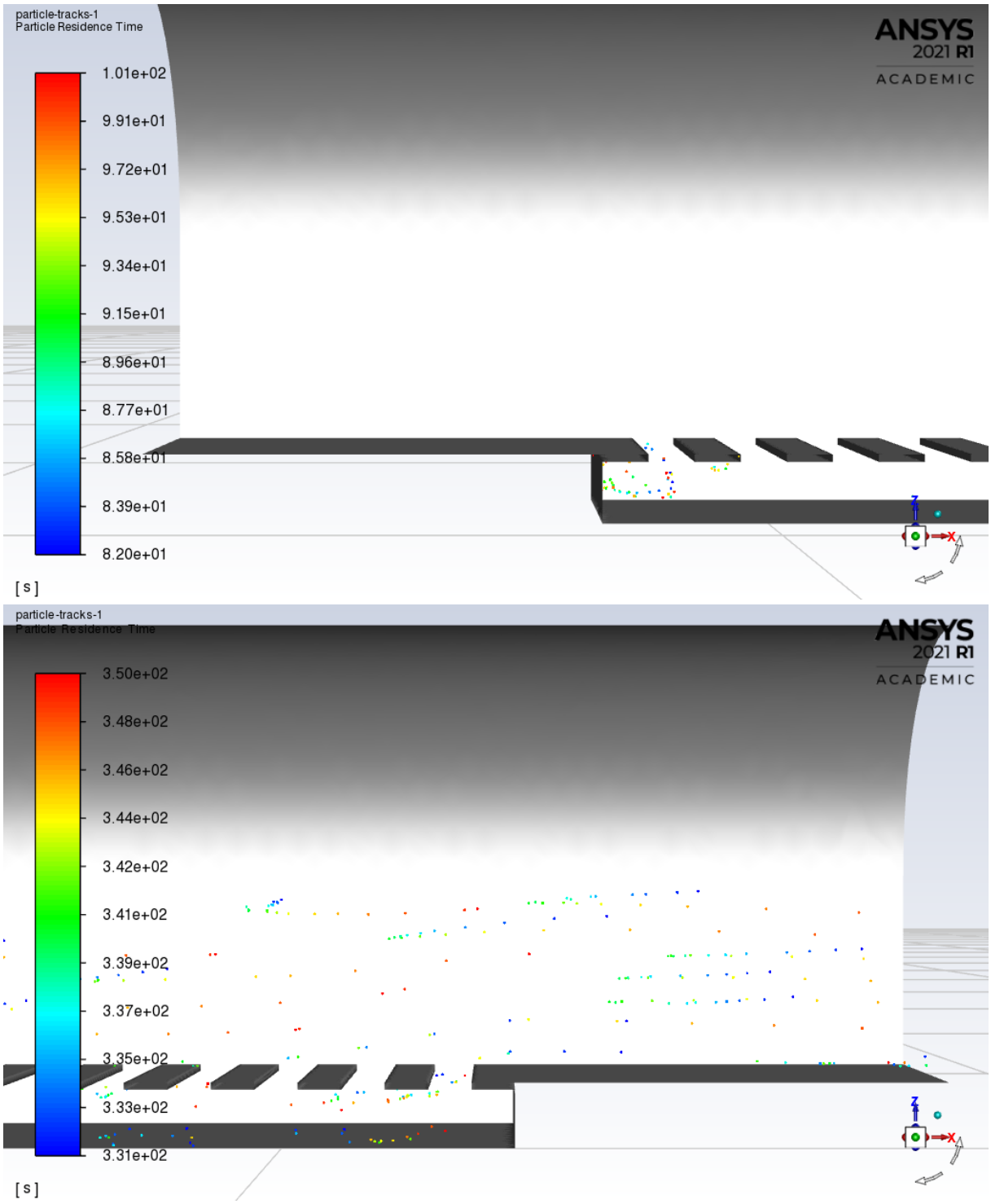

Figure 5.6: Injection of 0.1 mm particles at 350 s.

5.2 Testing cases: Variable rib and spacing widths

The results of the transient simulations where the rib width is equal to the opening between the ribs are presented in figure 5.7. The results of the transient simulations where the rib width is fixed at 1 m and the opening between the ribs is changed are presented in figure 5.8.

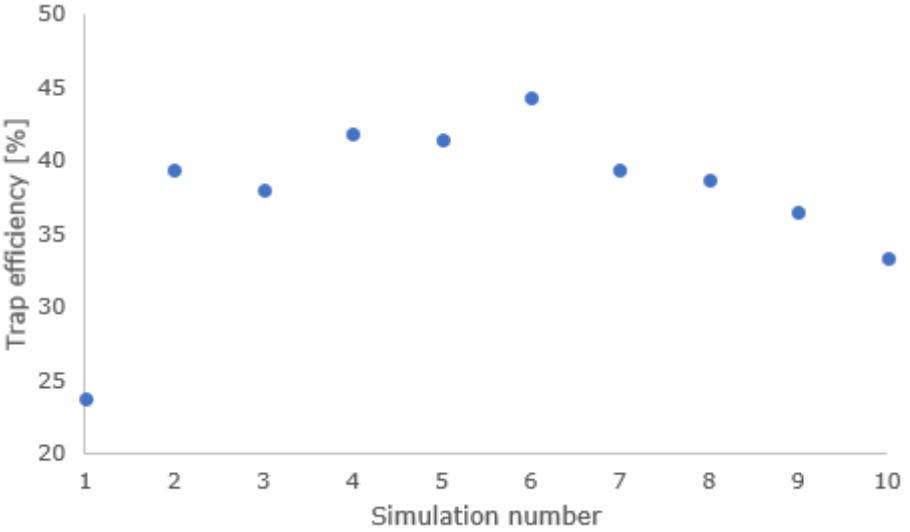

Figure 5.7: Trap efficiency when rib width is equal to rib opening.

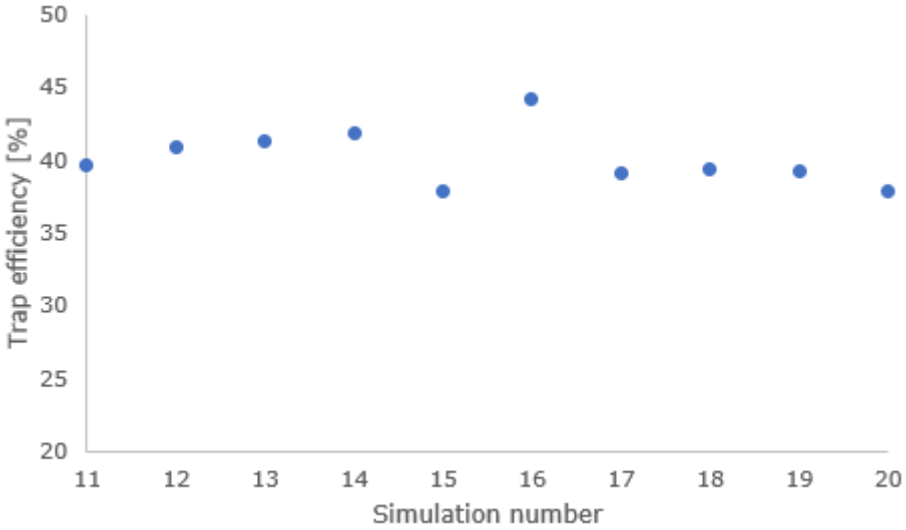

Figure 5.8: Trap efficiency when rib width is 1 m and opening varies.

6 Discussion

The results from the figures describing the flow through the sandtrap in section 5.1 show that turbulent areas and recirculation zones affect the settling of particles. The recirculation zone under the first rib has a lower impact on the trap efficiency owing to its location far upstream the outlet, and particles escaping the zone is most likely trapped before reaching the outlet. The recirculation zone under the last rib has a negative impact on the trap efficiency, as particles are lifted from the volume under the ribs into the main flow, allowing them to escape. The comparison between the CFD and the physical model in section 4.7.1 showed that the velocity under the ribs was higher for the CFD model compared with the physical model. Increased velocity under the ribs is associated with bad conditions for particle settling, as sediments will more easily be transported with the flow also below the ribs. Higher velocity may also increase the impact of the recirculation zones at the first and last ribs. The same flow behavior was observed for all the simulations.

For the simulations where the rib width is equal to the opening between the ribs, the setup with 1 m by 1 m ribs resulted in the highest trap efficiency, 44.2%. Simulations 2, 3 and 4 have a less decreasing trend compared to simulations 7, 8, 9 and 10, meaning narrower ribs and opening is better than larger ribs and opening for the trap efficiency. Simulation 1 resulted in a substantially lower trap efficiency, but confirms the sinking trend further away from the recommended setup in simulation 6. As described in section 4.8, the model had to be changed to cope with the limitations, and the procedure of simulation 1 was therefore different compared to the rest.

For the simulations where the rib width is kept at 1 m and the opening between the ribs is varied, the recommended setup with 1 m by 1 m ribs also resulted in the highest trap efficiency, 44.2%. The trap efficiency for the simulations with smaller opening than 1 m, is slightly higher than for simulations with a larger opening, with the exception for simulation 15. The reason for the drop in trap efficiency observed in simulation 3, 5 and 15 is most likely caused by uncertainty in the CFD solution, as a drop in between two higher results is not expected. For simulations 11-20, a decreasing trap efficiency is observed as the opening decreases/increases from the 1 m recommendation, but with a lower rate compared to the first 10 simulations.

Hypothesis 1: It is possible to improve the design of closed sandtraps

The results from the simulations showed that it was not possible to improve the trap efficiency with the two variables investigated in this thesis. However, other variables are expected to have potential to increase the trap efficiency. For example, vertical walls under each rib to stop the flow in the storage volume will allow for particles to settle in calm conditions and improve the trap efficiency. Increasing the roughness height of the tunnel invert, baffle walls can be installed under the ribs, thus improving settling conditions (Zenz & Richter, 2020). Another potential for improvement is the design and shape of the rib itself. Sharp edges at the upstream and downstream part of the rib produce turbulence between the ribs, and optimizing the shape can improve particle settling (Havrevoll et al., 2021). The angle of the rib referred to the flow direction can also have an impact on the trap efficiency. Particles can temporarily settle on top of the

ribs, and depending on the flow, they can either be transported further downstream or fall in between the ribs. A chamfer shape or angle on the ribs can allow the particles to fall into the storage volume with a reduced chance of getting resuspended into the flow. However, for the two tested variables in this work, no improvement was found.

Hypothesis 2: The optimum distance between ribs is 0.5 m.

The variables tested in the simulations discovered that the optimal rib width was 1 m with the chosen numerical approach. The results showed that the trap efficiency was higher for all simulations with an opening between the ribs smaller than 1 m, compared to a larger opening. As mentioned earlier, several variables can be tested to improve the trap efficiency, and with a different numerical approach, a smaller distance between the ribs may improve the particle settling. The results from simulation 3 and 13 with 0.5 m opening obtained a trap efficiency of 37.9% and 41.3%, respectively. Simulation 3 had a slightly lower trap efficiency than its coherent setups, which mentioned earlier may be caused by the uncertainty in the CFD solution. The results did not confirm the hypothesis regarding the opening of 0.5 m, but they clearly show that a smaller gap between the ribs provide a higher trap efficiency compared to larger gaps, for both variables. The higher trap efficiency may be a result from the smaller openings better separating the main flow from the storage volume, as proposed in the justification for the hypotheses.

The injections used in the simulations consisted of particles with 0.1 mm diameter injected from a surface 5 m upstream the rib section. Closed sandtraps are generally designed to trap the sediments transported as bed load, meaning particles in the range d > 0.3 -0.6 mm depending on velocity (Eggen, 1973). The particles injected in the simulations can be classified as suspended load, and as mentioned in section 2, sufficiently long sandtraps can expect to trap some of the sediments transported in suspension. Since the particles are transported in suspension, they are heavily affected by turbulence and flow pattern, and a large quantity of the particles follow the main flow. For larger particles transported as bed load, the opening between the ribs can then be decreased to a minimum to protect the storage volume from the main flow. However, the gap between the ribs cannot be too small, as theoretically, particles can hit every rib through the sandtrap and escape. Based on the results from this work, 0.5 m distance between the ribs was not found to be an improvement to the 1.0 m distance from the reference case.

Hypothesis 3: The optimum width of each rib is 1.0 m.

Regarding the optimum width, the results showed that the simulation with 1.0 m by 1.0 m had the best trap efficiency. The average trap efficiency for the two different design criteria is 39.1% for simulations 2-10 and 40.1% for simulations 11-20. Owing to the uncertainty of the CFD model, the results must be interpreted with care, but as mentioned earlier, the decreasing trap efficiency has a lower rate for the simulations with 1.0 m wide ribs. However, it cannot be concluded that 1.0 m is the optimum width of a rib, owing to the number of simulations run in proximity of 1.0 m. The closest widths used in the simulations were 0.75 m and 2.0 m, leaving a large span of rib widths not tested. Simulations where the rib widths are decreased and increased with shorter intervals to the 1.0 m setup is required to draw conclusions, even for the variables tested in the setup used for the simulations in this thesis.

The results from the simulations for both design criteria, reveal that the highest trap efficiency for the 0.1 mm particle injection is obtained with the current design

recommendation of 1 m wide ribs with 1 m opening. The trap efficiency is decreasing when moving away from the 1 m by 1 m setup for both criteria. For the numerical methods applied in this thesis the optimal rib design is the original recommendation of 1 m wide ribs with 1 m opening.

Simulation setup

A substantial amount of sediments are transported from the storage volume into the main flow by the recirculation zone under the last rib, exemplified by figure 5.6. This was observed in all simulations but was not quantified. Variations in the number of particles escaping from the storage volume between the simulations may have large effects on the trap efficiency. Measures to calm the flow by the last rib could greatly affect the efficiency of the sandtrap and should be further investigated.

The mesh used for the simulations is the finest that can be applied within the limitations of the academic license of Ansys Fluent. A mesh independence study could be performed to investigate how increasing the number of cells influence the trap efficiency and the uncertainty of the model. Since the mesh is made with the maximum number of cells allowed, a mesh independence study is not possible to perform for a finer mesh, only for coarser ones. The results from the simulations show several drops in the trap efficiency which can be caused by the sensitivity of the mesh. A new mesh was created for every simulation and experimenting with cell sizes was necessary to stay under the limitation. Simulations with a commercial license without a limitation could investigate the effect of a finer mesh.

The turbulence was modelled with Reynolds-Averaged Navier-Stokes (RANS). The method uses time-averaged values of fluctuations in for example velocity, to describe the average effect of turbulence, compared to solving the turbulent fluctuations. More accurate results can be found by applying more computationally demanding turbulence models such as Large Eddy Simulations (LES). Accurate calculation of turbulence is important due to the particles being mostly suspended load. Detailed calculation of turbulence could also reveal the impact of the recirculation zones to see the severity of lifting particles from under the ribs to the main flow.

The simulations were carried out using First Order Upwind scheme (FOU), despite Second Order Upwind scheme (SOU) being regarded as more accurate. For the numerical setup used in this thesis, the turbulent kinetic energy failed near the ribs when using the second order discretization scheme. The reason could be linked to how the SST k-ω turbulence model adapts to the ribs as they are modelled as walls, and the model is transformed to a k-ε model as described in section 4.6.3. Different turbulence models were not applied and could provide better conditions for the second order scheme. The k and ω converged well with the first order scheme which means the turbulent energy is calculated with good accuracy.

For the discrete phase boundary conditions on the walls and ribs, the coefficient of restitution is set to a value of 0.9 for both the tangential and the normal direction. These values are based on experience. For the bed, the *trapped* boundary condition terminates the calculation after a particle has hit the bed. In a real-world scenario, turbulent flow might lift particles settled on the bed and transport them further downstream, where they eventually might escape.

7 Conclusion

In this thesis, CFD simulations of a closed sandtrap were performed to investigate how the ribs affect the trap efficiency of the sandtrap. The simulations were carried out using the academic version of the CFD program Ansys Fluent. The main objective of the thesis was to investigate three hypotheses concerning rib design:

1. *It is possible to improve the design of closed sandtraps.*
2. *The optimum distance between the ribs is 0.5 m.*
3. *The optimum width of each rib is 1.0 m.*

Steady-state Reynolds-Averaged Navier-Stokes simulations were carried out with two different discharges to calibrate the CFD model with the physical model in the hydraulic lab. The velocity around the ribs in the control region showed good correlation between the CFD model in prototype scale and the physical model of sandtrap no. 3 in Tonstad hydropower plant in 1:20 scale.

Transient Reynolds-Averaged Navier-Stokes simulations with injections of 0.1 mm sediments were performed to test the effect of different rib designs. In total, 20 transient simulations were performed with 10 simulations per design approach. For both approaches, the rib setup that provided the best trap efficiency was the case with 1 m wide ribs with 1 m opening between the ribs that resulted in 44.2% trap efficiency.

1. It was found that it was not possible to improve the design of closed sandtraps with the variables investigated in this thesis.
2. The optimal distance between the ribs is 1 m with the numerical setup used in this thesis.
3. It was found that the optimal width is 1 m with the variables investigated in this thesis. However, it was not performed enough simulations in near proximity to 1.0 m to conclude on an optimum width.

It was found that the recommended rib design presented in the literature review could not be improved with the alternative designs tested in this thesis. The results show that minimizing the gap between the ribs is positive for the trap efficiency, by protecting the storage volume from the main flow. The simulation results from this work confirm the physical model studies performed in the hydraulic laboratory in the 1960s referenced by Eggen (1973), that is the basis for current state-of-the-art design recommendations.

7.1 Proposals for future work

The work conducted with this thesis revealed several interesting topics for future work. The proposals are presented in the following list before a detailed description below.

- Perform simulations with the commercial version of Ansys Fluent to avoid limitations.
- Apply different numerical methods to make simulations with Second Order Upwind scheme possible.

- Use Large Eddy Simulations (LES) or other more computationally demanding models to simulate the turbulence with greater accuracy.
- Investigate measures to dampen the effect of the recirculation zone at the last rib.
- Investigate a design with vertical walls below each rib to stop the flow below the ribs.
- Numerical simulations of the rib width and opening in a closer proximity to the optimum design of 1.0 m.
- Perform simulations to observe the change in trap efficiency when the angle of the ribs toward the flow direction is varied.
- Perform simulations where the Discrete Phase boundary condition at the bed is set to *reflect*.
- Use a non-uniform particle diameter distribution to simulate the expected sediment sizes transported into the sandtrap.

Future investigations of rib design should be performed with the commercial version of Ansys Fluent to investigate the sensitivity of the mesh, and the effect on the simulation results. Avoiding the limitations in the academic version would allow for a finer mesh without the need to adjust the minimum cell size needed in this thesis. Furthermore, testing of different numerical methods could allow for the use of Second Order Upwind scheme that may lead to higher accuracy of the results.

In this thesis it was observed a recirculation zone at the last rib that transported a significant quantity of sediments from under the ribs to the outlet. Simulations with a higher accuracy turbulence model such as LES could improve the solution and investigate the severity of the recirculation zone. Measures to decrease the effects of the recirculation zone could be necessary. Investigating how increasing the width of the last rib affects the backflow or installing vertical walls under each rib to stop the flow under the ribs completely, could greatly improve settling conditions.

The results showed that the optimum design was the 1 m by 1 m recommendation. Furthermore, performing simulations where the rib width and opening are varied in a closer proximity to the 1 m by 1 m design, and investigating how the angle of the ribs affect the trap efficiency, to see if there exists an optimized design. Simulations with non-uniform particle distribution together with *reflect* boundary condition for the bed could predict the particle movement and filling of the sandtrap.

8 References

AIAA (1998). *Guide for the Verification and Validation of Computational Fluid Dynamics Simulations*. AIAA G-077-1998.

Almeland, S. K., Olsen, N. R. B., Bråtveit, K. & Aryal, P. R. (2019). *Multiple solutions of the Navier-Stokes equations computing water flow in sand traps.* Engineering Applications of Computational Fluid Mechanics, 13(1): 199-219.

Ansys Fluent, *Ansys Fluent Theory Guide.* Ansys Fluent 2021 R1.

Brevik, O. (2013). *3D Numerisk modellering av deler av vannvegen til Tonstad kraftverk.* MSc. thesis. Trondheim: NTNU, Department of Hydraulic and Environmental Engineering

Bråtveit, K & Olsen, N. R. B. (2015). *Calibration of Horizontal Acoustic Doppler Current profilers by three dimensional CFD simulations.* Engineering Applications of Computational Fluid Mechanics, 9(1): 41-49.

Çengel, Y. A. & Cimbala, J. M. (2010). *Fluid Mechanics, Fundamentals and Applications.* (2nd ed.). McGraw-Hill Education.

Eggen, A. (1973). *Sandtransport og sandfang i kraftverkstunneler.* Trondheim: NTH, Vassdrags- og havnelaboratoriet.

Fergus, T., Hoseth, K. A. & Sæterbø, E. (2010). *Vassdragshåndboka.* Tapir Akademisk Forlag, Trondheim.

Guttormsen, O. (2018). *Vassdragsteknikk II.* Akademika Forlag, Trondheim.

Havrevoll, O. H., Vereide, K., Rüther, N. & Lia, L. (2021). *PIV experiments on ribs in the Tonstad rock trap model.* Trondheim: NTNU, Department of Civil and Environmental Engineering.

Lysne, D. K. (1967). *Sandtransport i tunneler.* Trondheim: NTH, Vassdrags- og havnelaboratoriet.

Lysne, D. K. (1969). *Movement of sand in tunnels.* Journal of the Hydraulics Division, 95(6): 1835-1846.

Mattimoe, J. J., Tinney, E. R. & Wolcott, W. W. (1964). *Rock trap experience in unlined tunnels*. Journal of the power division, proceedings of the American Society of Civil Engineers.

Menter, F.R., Kuntz, M. & Langtry, R. (2003). Ten Years of Industrial Experience with the SST Turbulence Model. In K. Hanjalić, Y. Nagano & M. Tummers (Eds.), *Turbulence, Heat and Mass Transfer 4*:625-632. Begell House.

Næss, R. (2020). *CFD Simulations of Open and Closed Sand Trap Design for Tonstad Hydropower Plant.* MSc. thesis. Trondheim: NTNU, Department of Civil and Environmental Engineering.

Olsen, N. R. B. (2017). *Numerical Modelling and Hydraulics.* (5th ed.). Trondheim: NTNU, Department of Hydraulic and Environmental Engineering.

Olsen, N. R. B. & Skoglund, M. (1994). *Three-dimensional numerical modeling of water and sediment flow in a sand trap.* Journal of Hydraulic Research, 32(6): 833-844.

Paschmann, C. (2018). *Design optimization of desanding facilities for hydropower schemes.* Zurich: ETH Zurich.

Patankar, S. V. (1980). *Numerical Heat Transfer and Fluid Flow.* New York, McGraw-Hill Book Company.

Ranga Raju, K. G., Kothyari, U. C., Srivastav, S. & Saxena, M. (1999). *Sediment Removal Efficiency of Settling Basins.* Journal of Irrigation and Drainage Engineering, 125(5): 308-314.

Richter, W., Mauko, G. & Zenz, G. (2020) *Flexible Sandtrap (FlekS) 2.0 Project extension.* TU Graz, Institute of Hydraulic Engineering and Water Resources Management.

Richter, W., Vereide, K. & Zenz, G. (2017). *Upgrading of Sand Traps in Existing Hydropower Plants*. Geomechanics and Tunnelling 10(5): 620-624.

Schwimmer, R. (2007). Accessed: 07.06.2021. https://serc.carleton.edu/NAGTWorkshops/sedimentary/activities/14100.html

Tvinnereim, K. (1980). Sandtransport og sandfang i kraftverkstunneler. *Eeu-kurs: Hydromekanikk i praksis.* Trondheim: NTH, Vassdrags- og havnelaboratoriet.

Vereide, K., Richter, W., Lia, L., Havrevoll, O. H. & Jakobsen, T. (2017). *Upgrading of Sand Traps in Existing Hydropower Plants.* Trondheim, NTNU.

Vereide, K., Richter, W., Havrevoll, O. H., Belete, K., Shrestha, U., Navaratnam, U., Mauko, G. & Lia, L. (2021). *Flexible Sandtraps Final Report.* Norwegian Research Centre for Hydropower Technology.

Versteeg, H. K. & Malalasekera, W. (2007). *An Introduction to Computational Fluid Dynamics: The Finite Volume Method* (2nd ed.). Pearson Education Limited.

Zenz, G. & Richter, W. (2020). *Flexible Sandtrap (FlekS) 1.0*. TU Graz, Institute of Hydraulic Engineering and Water Resources Management.

Appendices

Appendix A

Construction drawing used to create the geometry of the CFD model.

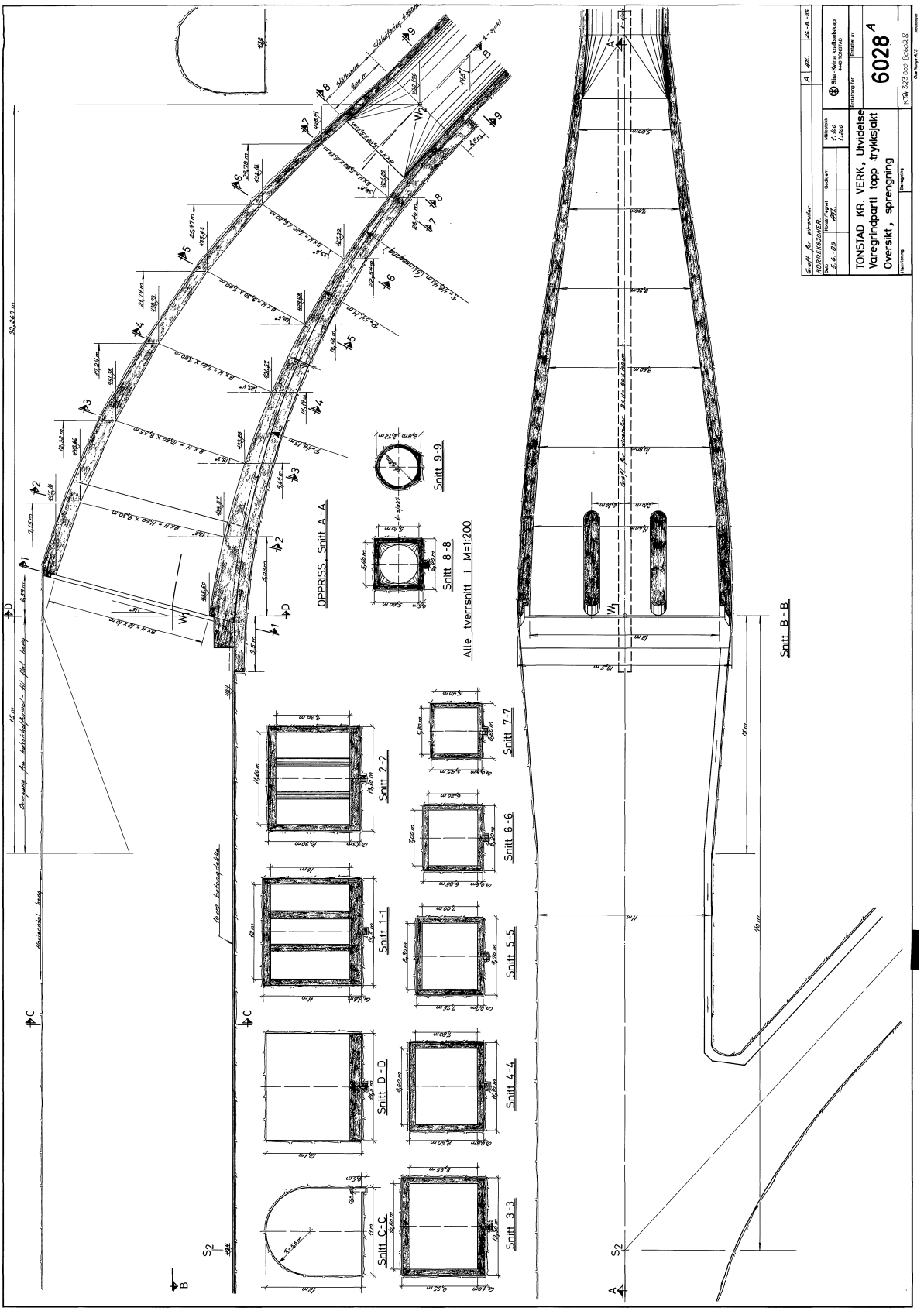
OPPRISS, Snitt A-A
Alle tverrsnitt i M=1:200
Snitt 9-9
Snitt 8-8
Snitt 7-7
Snitt 6-6
Snitt 5-5
Snitt 4-4
Snitt 3-3
Snitt 2-2
Snitt 1-1
Snitt C-C
Snitt D-D
Snitt B-B
TONSTAD KR. VERK, Utvidelse
Varegrindparti topp trykksjakt
Oversikt, sprengning
6028 A
Sira-Kvina kraftselskap
4440 TONSTAD

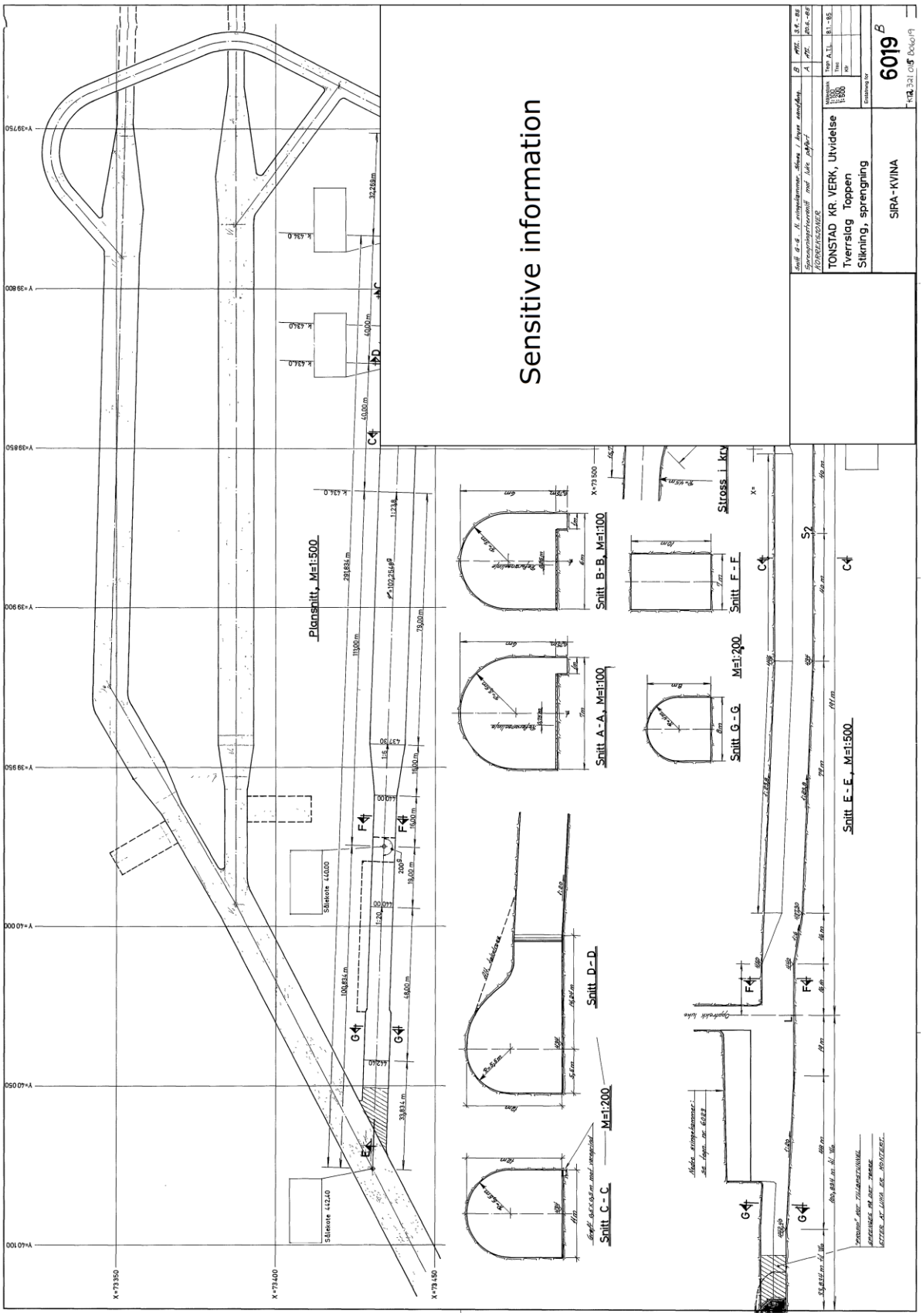
Sensitive information
TONSTAD KR. VERK, Utvidelse
Tverrslag Toppen
Stikning, sprengning
SIRA-KVINA
6019
Plansnitt, M=1:500
Snitt A-A, M=1:100
Snitt B-B, M=1:100
Snitt C - C
M=1:200
Snitt D-D
Snitt E-E, M=1:500
Snitt F - F
Snitt G - G
M=1:200
Stross i kry
Sålekote 440.00
Sålekote 442.40

Appendix B

A folder with videos showing the particle tracks for some of the simulations are attached.

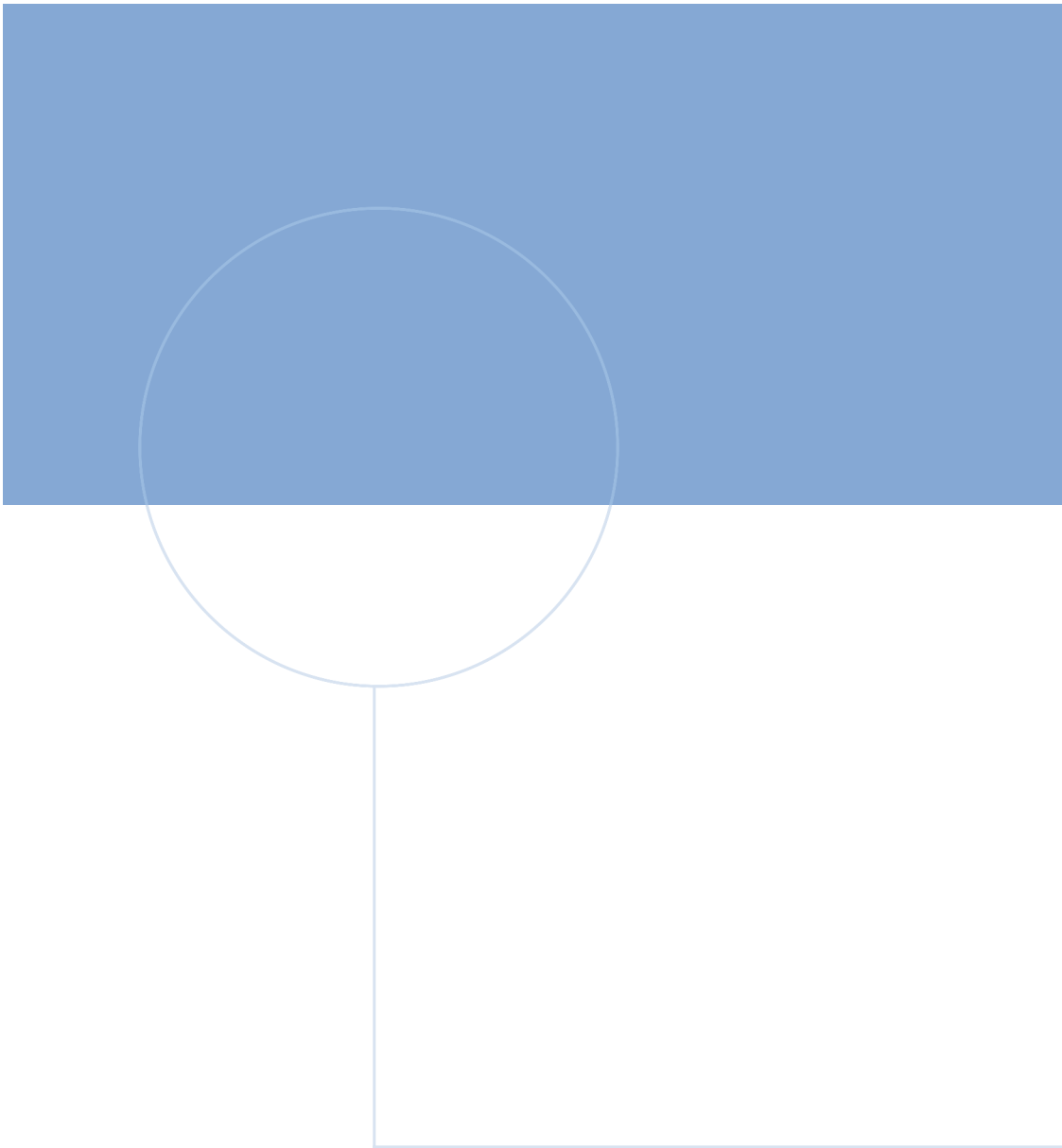

NTNU

Norwegian University of
Science and Technology